J. Fluid Mech. (2009), *vol.* 618, *pp.* 209–241. © 2008 Cambridge University Press
doi:10.1017/S0022112008004345 Printed in the United Kingdom

Receptivity mechanisms in three-dimensional boundary-layer flows

LARS-UVE SCHRADER, LUCA BRANDT† AND DAN S. HENNINGSON

Linné Flow Centre, KTH Mechanics, SE-100 44 Stockholm, Sweden

(Received 21 January 2008 and in revised form 10 September 2008)

Receptivity in three-dimensional boundary-layer flow to localized surface roughness and free-stream vorticity is studied. A boundary layer of Falkner–Skan–Cooke type with favourable pressure gradient is considered to model the flow slightly downstream of a swept-wing leading edge. In this region, stationary and travelling crossflow instability dominates over other instability types. Three scenarios are investigated: the presence of low-amplitude chordwise localized, spanwise periodic roughness elements on the plate, the impingement of a weak vortical free-stream mode on the boundary layer and the combination of both disturbance sources. Three receptivity mechanisms are identified: steady receptivity to roughness, unsteady receptivity to free-stream vorticity and unsteady receptivity to vortical modes scattered at the roughness. Both roughness and vortical modes provide efficient direct receptivity mechanisms for stationary and travelling crossflow instabilities. We find that stationary crossflow modes dominate for free-stream turbulence below a level of about 0.5 %, whereas higher turbulence levels will promote the unsteady receptivity mechanism. Under the assumption of small amplitudes of the roughness and the free-stream disturbance, the unsteady receptivity process due to scattering of free-stream vorticity at the roughness has been found to give small initial disturbance amplitudes in comparison to the direct mechanism for free-stream modes. However, in many environments free-stream vorticity and roughness may excite interacting unstable stationary and travelling crossflow waves. This nonlinear process may rapidly lead to large disturbance amplitudes and promote transition to turbulence.

1. Introduction

The classical transition path to turbulence in laminar boundary-layer flow is characterized initially by the receptivity phase, i.e. the conversion of external perturbations into boundary-layer disturbances, subsequently by linear and nonlinear growth of the disturbances and finally by the breakdown to turbulence via secondary instability. Despite the fact that the linear amplification of the unstable waves can now be accurately estimated, reliable values for the initial condition of these perturbations must be provided. Commonly used industrial transition-prediction tools, e.g. the e^N-method, exclude the receptivity phase. In order to overcome the need to 'guess' the initial disturbance conditions, receptivity has previously been studied analytically, experimentally and numerically.

† Email address for correspondence: luca@mech.kth.se

https://doi.org/10.1017/S0022112008004345 Published online by Cambridge University Press

1.1. *Receptivity of Blasius flow*

The foundation of receptivity studies had already been laid in the 1980s by Goldstein (1983, 1985) and Ruban (1985), who employed asymptotic analysis to investigate receptivity at the first neutral point of Tollmien–Schlichting (TS) instability in Blasius flow. They pointed out that resonance regarding frequency and wave vector between the external disturbances and the unstable eigenmode of the base flow is necessary to trigger boundary-layer instability. The excitation of TS waves, for instance, requires unsteady external perturbations, e.g. acoustic or vortical free-stream disturbances. However, free-stream perturbations feature in general larger chordwise wavelengths than the discrete eigenmodes of the mean flow. Hence, scale reduction is necessary to trigger TS instability by free-stream disturbances. Goldstein (1985) shows that scale conversion requires a short-scale downstream variation of the base flow. This requirement is fulfilled in two regions: just downstream of the leading edge where the boundary layer grows rapidly, and in the vicinity of a localized surface non-uniformity. Thus, two different receptivity mechanisms to unsteady free-stream perturbations are imaginable: (i) a direct process in the leading-edge region, associated with the unsteady free-stream disturbance, and (ii) a mechanism associated with the interaction between unsteady free-stream perturbations and the steady disturbance induced by localized surface non-uniformity. For acoustic free-stream perturbations only the second receptivity mechanism proved to be efficient.

1.2. *Receptivity of three-dimensional boundary layers*

Three-dimensional boundary layers can be found on swept wings or blades and are therefore of importance in aeronautics and turbomachinery. In particular, the flow over a swept flat plate subject to a chordwise pressure gradient has often been considered in the literature. This is a prototype for swept wings, being referred to as a Falkner–Skan–Cooke boundary layer. Most studies focus on crossflow instability waves, since they dominate the perturbation scenario inside the boundary layer, given a large sweep angle. In contrast to TS instability, crossflow instability is of the inviscid type and can be stationary as well as travelling.

Results on receptivity and stability in three-dimensional boundary-layer flow have been reviewed by Saric, Reed & White (2003). In the 1990s, the finite reynolds-number theory (FRNT), originally developed by Zavol'skii, Reutov & Ryboushkina (1983) for two-dimensional boundary layers, has been addressed by e.g. Crouch (1993), Choudhari (1994) and Ng & Crouch (1999). In contrast to asymptotic analysis, FRNT is valid for moderate Reynolds numbers and can be applied upstream and downstream of the first neutral point of the instability. It is based on perturbation equations of Orr–Sommerfeld/Squire type and incorporates in its usual formulation the parallel-flow assumption. External disturbances are included in finite Reynolds-number theory as non-homogeneous boundary conditions, e.g. for wall roughness, or as an additional forcing term, e.g. for acoustic free-stream waves. Finite Reynolds-number theory further assumes that the excited boundary-layer disturbances are convective in nature. The work by Crouch (1993) and Choudhari (1994) deals with Falkner–Skan–Cooke boundary-layer flow exposed to both surface non-uniformities and acoustic free-stream perturbations. These authors consider linear receptivity to localized small-amplitude roughness elements, exciting steady crossflow instability, and an unsteady receptivity mechanism due to a weak planar acoustic free-stream wave scattered at the roughness, generating travelling crossflow modes. They characterize the receptivity process by an efficiency coefficient, which relates the initial amplitude of the instability mode to that of the triggering perturbations. Although Crouch (1993)

https://doi.org/10.1017/S0022112008004345 Published online by Cambridge University Press

and Choudhari (1994) found higher efficiency for the unsteady receptivity mechanism, the steady receptivity process to roughness gave larger initial disturbance amplitudes. This is due to the interaction of two small-amplitude disturbances in the case of unsteady receptivity. They concluded therefore that stationary crossflow vortices are more likely to dominate transition in swept-wing flow under flight conditions than travelling crossflow instability.

Ng & Crouch (1999) and Collis & Lele (1999) consider receptivity to localized roughness of flow over a swept parabolic cylinder. While the former authors use this configuration as base flow for a FRNT study, Collis & Lele (1999) perform both non-parallel FRNT calculations and direct numerical simulations based on linearized perturbation equations. Spatial evolution of the boundary layer and surface curvature are included in their work. They found that non-parallel effects attenuate steady receptivity, while convex curvature enhances it. As in Crouch (1993) and Choudhari (1994), the most efficient receptivity sites were found slightly upstream of the first neutral point of the triggered stationary instability. Also Bertolotti (2000) studied the effect of non-parallel mean flow on receptivity to localized roughness for swept-wing flow. He emphasizes that non-parallel effects are substantial especially in the leading-edge vicinity. This is, on the one hand, due to rapid boundary-layer growth, on the other hand to highly curved streamlines in this region. Bertolotti performs his analysis in Fourier space, expanding to first order the base flow and the disturbance in the streamwise coordinate about the roughness location. The receptivity amplitude is then expressed as the sum of a zeroth- and a first-order contribution, and two separate efficiency coefficients are introduced. While the zeroth-order part resembles the formulation for the receptivity amplitude in finite Reynolds-number theory, the first-order contribution also involves the derivative of the Fourier amplitude of the roughness with respect to the instability wavenumber. Bertolotti (2000) found that non-parallel effects attenuate roughness receptivity, as well.

1.3. *Receptivity to vortical free-stream disturbances*

The numerical studies mentioned above are limited to acoustic free-stream disturbances. In turbomachinery, for instance, vortical perturbations in the free stream are often more relevant. Experimental work has been done on receptivity and transition of three-dimensional boundary layers subject to vortical free-stream disturbances, for instance by Bippes & Deyhle (1992) and Reibert *et al.* (1996). Also these studies revealed that steady crossflow disturbances dominate the boundary-layer response at the typically low turbulence levels under flight conditions. However, this may not be the case in noisy environments and for wind-tunnel tests, see Saric *et al.* (2003).

Although receptivity of three-dimensional boundary-layer flow to free-stream vortices has not been much studied, many publications on numerical and experimental studies of two-dimensional boundary layers subject to vortical free-stream disturbances are available; see for example Bertolotti & Kendall (1997), Kendall (1998), Jacobs & Durbin (1998, 2001), Brandt, Schlatter & Henningson (2004), Fransson, Matsubara & Alfredsson (2005) and the review by Saric, Reed & Kerschen (2002). Buter & Reed (1994) consider two-dimensional flow past a flat plate with an elliptic leading edge, exposed to time-periodic spanwise free-stream vortices. They found a receptivity mechanism for TS instability, which is, however, weaker than acoustic receptivity studied by Lin, Reed & Saric (1992) for the same configuration. The receptivity process becomes completely different, when the free-stream perturbations contain also streamwise vorticity. Then, the key structures

https://doi.org/10.1017/S0022112008004345 Published online by Cambridge University Press

prior to transition are no longer TS waves, but streamwise streaks of alternating high- and low-momentum fluid. The formation of the streaky pattern is due to the interaction between non-normal eigenmodes of the base flow. Bertolotti (1997) found for Blasius flow that maximum receptivity is obtained for free-stream vortices with zero streamwise wavenumber. He suggests a linear receptivity mechanism, by which the free-stream vortices diffuse into the boundary layer close to the leading edge and cause the formation of the streaks inside it. This process has been confirmed by Bertolotti & Kendall (1997) in an experiment with controlled free-stream conditions through the generation of a weak axial vortex by a micro wing upstream of a flat plate with elliptic leading edge. Although its core was located outside the boundary layer, the streamwise vortex was able to produce a rather strong perturbation inside it. The work also includes results from a numerical model of this flow configuration, and good agreement between the measured and the numerically determined amplitude function of the boundary-layer perturbation has been found. Berlin & Henningson (1999) consider both streamwise modes and a pair of oblique waves in the free stream. Apart from the linear receptivity mechanism, being efficient only for streamwise free-stream vorticity, they also found a nonlinear receptivity mechanism due to the interaction of two streamwise or two oblique free-stream vortices. Jacobs & Durbin (1998) suggest an alternative model for vortical free-stream disturbances in Blasius flow, based on the concept of the continuous spectrum of the Orr–Sommerfeld/Squire operator. They show that penetration of the vortical mode into the boundary layer is crucial for receptivity and that deepest penetration is obtained for low-frequency free-stream vorticity at low Reynolds numbers. The model of Jacobs & Durbin (1998) is used by Brandt, Henningson & Ponziani (2002) and compared with the oblique-mode model of Berlin & Henningson (1999). These authors found similar nonlinear receptivity mechanisms for both types of free-stream disturbance. To obtain a more realistic model for turbulence in the outer flow, Jacobs & Durbin (2001) and Brandt *et al.* (2004) consider the superposition of a large number of modes from the continuous Orr–Sommerfeld/Squire spectrum, weighted to obtain a typical energy-density spectrum of isotropic turbulence. For free-stream turbulence dominated by low frequencies, the linear receptivity mechanism was found to be the main cause of streak generation, whereas receptivity to high-frequency free-stream turbulence is characterized by the nonlinear mechanism. Zaki & Durbin (2005) show that bypass transition can be observed in numerical simulations, if only two vortical free-stream modes are prescribed at the inflow: one of low and one of high frequency. Whereas the low-frequency mode is responsible for the generation of streaks, the high-frequency mode triggers secondary instability upon the streaky flow.

The influence of streamwise pressure gradient on receptivity and transition in the presence of free-stream vorticity was investigated in Zaki & Durbin (2006) by direct numerical simulation of two-dimensional boundary-layer flow subject to a Falkner–Skan pressure distribution. That work also includes a study of the interaction between the continuous-spectrum modes and the boundary layer in Falkner–Skan flow, as has been presented by Maslowe & Spiteri (2001). Zaki & Durbin (2006) found that the free-stream modes penetrate less under adverse and more under favourable pressure gradient into the boundary layer than in Blasius flow; nonetheless, transition onset and completion are moved upstream for the former, and downstream for the latter, pressure distribution. The authors conclude that deep penetration of the free-stream modes is not crucial for the receptivity process in two-dimensional boundary layers.

Receptivity mechanisms in three-dimensional swept-plate flow, however, are much less studied than in Blasius flow, as stated by Saric *et al.* (2003). Results from

https://doi.org/10.1017/S0022112008004345 Published online by Cambridge University Press

direct numerical simulations (DNS) with a spectral method are herein presented to characterize the receptivity of three-dimensional boundary layers. A spatial approach is employed, capturing non-parallel effects on receptivity owing to the streamwise evolution of the mean flow. The focus lies on crossflow vortices, as well. Two perturbations are considered: localized roughness elements at the wall and vortical disturbances in the free stream. Three receptivity mechanisms are investigated: steady receptivity to roughness, unsteady receptivity to free-stream vorticity and unsteady receptivity due to scattering of a vortical mode at a localized roughness element. The first two mechanisms depend on the amplitude of the roughness element and the free-stream-mode, respectively, while the third receptivity process involves the product of two disturbance amplitudes. The three mechanisms are characterized in terms of a receptivity coefficient as a measure for their efficiency.

The paper is organized in the following fashion. Section 2 discusses the base flow (2.1), the numerical method (2.2) and the modelling of the surface-roughness element and the vortical free-stream disturbance (2.3). Section 3 focuses on steady receptivity to localized surface roughness, and § 4 deals with direct unsteady receptivity to a vortical free-stream mode. The advection of single vortical modes along a plate with localized roughness defines the third receptivity process being investigated in § 5. In § 6, the efficiency of the receptivity processes for stationary and travelling crossflow instability is compared. The results are discussed and summarized in § 7.

2. Flow configuration and numerical approach

2.1. *Base flow*

The flow over a swept flat plate subject to a chordwise pressure gradient is considered, a frequently studied prototype for swept wings. The base flow is obtained through the solution of the three-dimensional time-dependent incompressible Navier–Stokes equations, initialized with the Falkner–Skan–Cooke similarity profiles. This type of flow includes most of the features of the flow over the wing – the chordwise pressure drop, the streamline curvature and the crossflow, but not the surface curvature. The pressure gradient and the curvature of the external streamlines are included in Falkner–Skan–Cooke flow by assuming the following free-stream velocity distribution,

$$U_\infty(x) \equiv \frac{U^*_\infty(x^*)}{U^*_\infty(x^*_0)} = \left(\frac{x^* + x^*_0}{x^*_0}\right)^m, \tag{2.1a}$$

$$W_\infty \equiv \frac{W^*_\infty}{U^*_\infty(x^*_0)} = \tan\phi_0 = \text{const}, \tag{2.1b}$$

where U and W are used for the chord- and spanwise mean velocity and starred quantities have physical dimensions. The exponent m denotes the flow acceleration, related to the frequently used Hartree parameter β_H via

$$m = \frac{\beta_H}{2 - \beta_H}. \tag{2.2}$$

The angle ϕ_0 is the sweep angle at the reference station x^*_0. Owing to the chordwise flow acceleration, the free-stream velocity vector is turned more and more into the x^*-direction downstream, forming a curved streamline. The external streamline is sketched in figure 1, where the Falkner–Skan–Cooke base-flow profiles are shown with the coordinate system adopted. In this figure, the mean flow is decomposed along the free-stream direction at x^*_0 rather than along the chord- and spanwise

https://doi.org/10.1017/S0022112008004345 Published online by Cambridge University Press

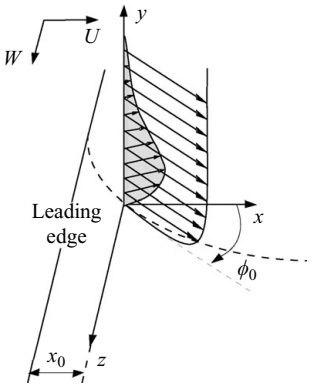


FIGURE 1. Wall-normal profiles of the streamwise and the crossflow velocity for Falkner–Skan–Cooke boundary-layer flow.

coordinates x^* and z^*. This decomposition shows a non-zero velocity in the cross-stream direction inside the boundary layer – the *crossflow*, resulting from a force imbalance between the pressure and the centrifugal forces. The crossflow profile exhibits an inflection point and supports inviscid instability, referred to as crossflow instability. Note that instability waves propagating in the direction of the crossflow have negative spanwise wavenumber β and positive chordwise wavenumber α in the chosen coordinate system.

The Falkner–Skan–Cooke boundary-layer flow is independent of the spanwise direction z^*, and is governed by the two-dimensional boundary-layer equations, see for instance Schlichting (1979). For the free-stream velocity distribution in (2.1), the boundary-layer equations for the chordwise and wall-normal mean velocities U^* and V^* can be re-arranged in a single equation by introducing the streamfunction $f(\eta)$, whereas the chordwise and the normal coordinate x^* and y^* can be replaced by one single similarity variable η,

$$\eta = \sqrt{\frac{m+1}{2}\frac{U_\infty^*(x^*)}{\nu^* x^*}}\, y^*. \tag{2.3}$$

If the spanwise velocity W^* is expressed as $W^* = W_\infty^* g(\eta)$, the boundary-layer equations can be transformed into a set of ordinary differential equations for $f(\eta)$ and $g(\eta)$,

$$f''' + ff'' + \beta_H(1 - f'^2) = 0, \tag{2.4a}$$

$$g'' + fg' = 0, \tag{2.4b}$$

with boundary conditions

$$\eta = 0: \qquad f = f' = g = 0, \tag{2.5a}$$

$$\eta \to \infty: \qquad f \to 1, \quad g \to 1. \tag{2.5b}$$

Self-similar profiles for the chordwise and the spanwise velocity U^* and W^* are obtained from $f'(\eta)$ and $g(\eta)$. They are referred to as the Falkner–Skan–Cooke similarity profiles in literature. Further details can be found in Schmid & Henningson (2001) or Högberg & Henningson (1998).

Throughout the remainder of this paper, non-dimensional variables are used. Lengths are made dimensionless by the chordwise boundary-layer displacement

https://doi.org/10.1017/S0022112008004345 Published online by Cambridge University Press

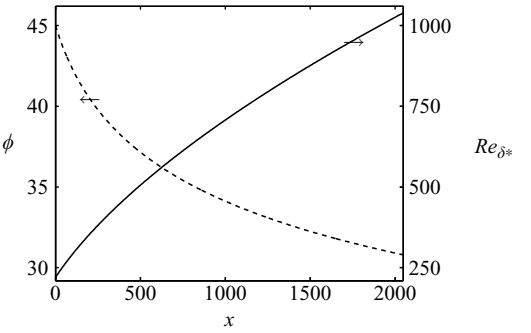


FIGURE 2. Reynolds number (——) and external streamline angle (---) as a function of the chordwise coordinate.

thickness $\delta_0^* \equiv \delta^*(x_0^*)$ at the reference location x_0^* and velocities by the chordwise free-stream velocity $U_{\infty,0}^* \equiv U_\infty^*(x_0^*)$. The dimensionless reference station x_0 is located downstream of the leading edge of the plate and corresponds to the inflow plane of the computational domain. The reference length δ_0^* and the reference velocity $U_{\infty,0}^*$ define the Reynolds number at the computational inlet,

$$Re_{\delta_0^*} = \frac{U_{\infty,0}^* \delta_0^*}{\nu^*}, \tag{2.6}$$

where ν^* is the kinematic viscosity. The local Reynolds number Re_{δ^*} is defined by replacing δ_0^* and $U_{\infty,0}^*$ in (2.6) by their local values $\delta^*(x)$ and $U_\infty^*(x)$. Figure 2 shows the relation between the local Reynolds number Re_{δ^*} and the chordwise coordinate x (solid line). Also the local angle ϕ of the external streamline is displayed versus x (dashed line).

The inflow Reynolds number is $Re_{\delta_0^*} = 220$ for most of the present results, corresponding to an inflow station at $x_0 = 167\delta_0^*$ downstream of the leading edge. The parameters m and ϕ_0 in (2.1) are chosen in order to obtain conditions similar to those of the airfoil experiments at Arizona State University by Reibert *et al.* (1996). These authors report among other results the N-factor of the steady crossflow instability wave with 12 mm spanwise wavelength at different chordwise stations. The local N-factor measured on the swept airfoil at 10 % chord is approximately obtained at the corresponding station on the swept flat plate, if $m = 0.2$, or $\beta_H = 0.333$, is selected. In addition, this value gives a chordwise free-stream velocity distribution, which matches sufficiently well the c_p distribution reported by Reibert *et al.* (1996). The sweep angle at x_0^* is set to $\phi_0 = 45°$, as in the experiment. The crossflow component is most pronounced at this angle, and the crossflow instability waves dominate over other types of instability. Also note that the streamwise and spanwise free-stream velocity are equal at the reference location for $\phi_0 = 45°$, i.e. $U_\infty(x_0) = W_\infty(x_0) = 1$.

2.2. *Numerical method*

The present results are obtained by means of a simulation code based on spectral methods to solve the three-dimensional time-dependent incompressible Navier–Stokes equations, see Chevalier *et al.* (2007). The algorithm builds on a Fourier representation along the chord- and spanwise coordinates x and z and on Chebyshev polynomials in the wall-normal direction y, together with a pseudo-spectral treatment of the nonlinear terms. The time integration is based on a four-step third-order Runge–Kutta method for the nonlinear terms and a second-order Crank–Nicolson scheme for the linear terms. Aliasing errors from the computation of the nonlinear terms are

https://doi.org/10.1017/S0022112008004345 Published online by Cambridge University Press

removed in wall-parallel planes by the 3/2-rule, whereas a grid refinement normal to the plate has turned out to be more convenient than dealiasing.

The swept-plate boundary layer develops along the chordwise direction, while the streamlines continuously change direction. For the simulation of such spatially evolving flows, the required chordwise periodicity is established by the implementation of a 'fringe region' at the downstream end of the computational domain, as described by Nordström, Nordin & Henningson (1999). In this region the velocity field $\mathscr{U}$ is forced to the desired velocity profiles $\mathscr{U}_0$ by an additional term in the Navier–Stokes equations. Here, $\mathscr{U}$ is used for the instantaneous velocity field to distinguish it from the base flow U. $\mathscr{U}_0$ indicates the desired inflow, i.e. the Falkner–Skan–Cooke similarity profiles, and may also contain incoming disturbances. The equation solved is,

$$\frac{\partial \mathscr{U}}{\partial t} = \mathscr{NS}(\mathscr{U}) + \lambda(x)(\mathscr{U}_0 - \mathscr{U}), \tag{2.7}$$

where $\mathscr{NS}$ denotes the right-hand side of the momentum equations, and $\lambda(x)$ is a smooth forcing function, being non-zero only in the fringe region.

Along the plate, no-slip conditions apply for the basic and the perturbed flow in the case of vortical free-stream perturbation, while non-homogeneous boundary conditions are employed to model the surface roughness, see § 2.3. At the free-stream boundary, a von Neumann condition is used for the computations with free-stream vortical modes, and the computational domain is chosen high enough to ensure independence of the boundary-layer response from the location of, and the conditions at, the top boundary. To compute the base flow and the disturbed flow in the case of surface roughness, the asymptotic condition proposed by Malik, Zang & Hussaini (1985) is employed,

$$y = y_\infty: \quad \frac{\partial \hat{\boldsymbol{u}}}{\partial y} + \sqrt{\alpha^2 + \beta^2}\,\hat{\boldsymbol{u}} = \frac{\partial \hat{\boldsymbol{U}}}{\partial y} + \sqrt{\alpha^2 + \beta^2}\,\hat{\boldsymbol{U}}. \tag{2.8}$$

This condition is equivalent to the requirement of zero vorticity at the free-stream boundary y_∞, allowing us to place it nearer the boundary layer, and it is applied in Fourier space, as indicated by the hat. $\boldsymbol{U}$ stands for the mean flow, $\boldsymbol{u}$ for the disturbance velocity and α and β for the chord- and spanwise wavenumber, respectively. As the mean flow is independent of, and the perturbed flow periodic in, the spanwise direction z, cyclic boundary conditions are applied along z.

The simulation code provides the possibility of solving the nonlinear and the linearized perturbation equations about any three-dimensional base flow. Herein, the linearized perturbation equations are solved for the studies of direct receptivity to roughness and free-stream vortices presented in the §§ 3 and 4 and the nonlinear equations for the unsteady receptivity problem to free-stream vorticity in combination with roughness described in § 5.

2.3. *Disturbance generation*

In the present paper, the receptivity of the three-dimensional swept-plate boundary layer is studied for two different types of external disturbances – steady roughness elements on the plate surface and unsteady vortical disturbance in the free stream. This section reports how these two types of disturbance are modelled and implemented in the simulation code.

https://doi.org/10.1017/S0022112008004345 Published online by Cambridge University Press

2.3.1. *Surface roughness*

A chordwise localized, spanwise periodic roughness element,

$$h(x, z) = \varepsilon_h \, h_x(x) \sin(\beta_R z), \tag{2.9}$$

is placed downstream of the inflow plane x_0. ε_h is a small parameter describing the maximum amplitude of the roughness bump, and $\beta_R = 2\pi/L_z$ is the spanwise wavenumber of the roughness bump. The spanwise length scale of the roughness element and the spanwise width L_z of the computational domain are hence identical. Roughness elements of different spanwise scales will be considered separately, owing to the assumption of linear flow behaviour and the spanwise homogeneity of the base flow. The chordwise shape $h_x(x)$ is

$$h_x(x) = \left[S\left(\frac{x - h_{start}}{h_{rise}} \right) - S\left(\frac{x - h_{end}}{h_{fall}} + 1 \right) \right], \tag{2.10}$$

where S is a smooth step function,

$$S(\xi) = \begin{cases} 0, & \xi \leqslant 0, \\ 1/\left(1 + \mathrm{e}^{(1/(\xi-1)+1/\xi)}\right), & 0 < \xi < 1, \\ 1 & \xi \geqslant 1. \end{cases} \tag{2.11}$$

The parameters h_{start}, h_{end}, h_{rise} and h_{fall} in (2.10) indicate the start and end station of the bump, i.e. $h_x(x) \neq 0$ on $[h_{start}, h_{end}]$, and the extension of the rising and the falling flank of the smooth step. The roughness element is not meshed, but modelled by non-homogeneous boundary conditions along the plate. The no-slip conditions along the bump contour $h(x, z)$ are projected from the bump surface to the undisturbed wall $y = 0$ via a Taylor series expansion,

$$\begin{pmatrix} u \\ v \\ w \end{pmatrix}_0 = \begin{cases} \begin{pmatrix} -h(x,z)\frac{\partial U}{\partial y} \\ 0 \\ -h(x,z)\frac{\partial W}{\partial y} \end{pmatrix}_{\mathbf{0}}, & h_{start} \leqslant x \leqslant h_{end}, \\ \mathbf{0}, & \text{elsewhere}, \end{cases} \tag{2.12}$$

where u, v and w are the components of the disturbance velocity. Since the roughness height ε_h is assumed to be small, the Taylor series is truncated at first order. The parameters used in (2.9) and (2.10) are specified when presenting the results in 3, where the model for roughness receptivity will be motivated in the context of previous studies reported in literature.

2.3.2. *Free-stream and boundary-layer modes*

The unsteady free-stream disturbance is modelled by adding a single vortical mode to the base flow in the fringe region. To analyse the effect of single waves of specific wavenumbers and frequencies, Fourier modes would be a natural choice. However, in the presence of the plate, the vortical mode has to decay smoothly to zero towards the wall. Eigenfunctions associated with the continuous wavenumber spectrum of the Orr–Sommerfeld/Squire operator for three-dimensional boundary-layer flows are therefore used to represent the free-stream modes, as for example in Jacobs & Durbin (1998) and Brandt *et al.* (2004). These continuous-spectrum eigenfunctions are sometimes also denoted *continuous modes*, while the eigenfunctions from the discrete wavenumber spectrum of the Orr–Sommerfeld/Squire operator are called *discrete modes*.

https://doi.org/10.1017/S0022112008004345 Published online by Cambridge University Press

Grosch & Salwen (1978) first introduced the concept of the continuous spectrum for the Orr–Sommerfeld/Squire operator by relaxing the free-stream boundary conditions at $y \to \infty$. The derivation is outlined here since it is presented for the first time for three-dimensional boundary layers. In the limit $y \to \infty$, the Orr–Sommerfeld/Squire system simplifies to a set of two decoupled homogeneous ordinary differential equations with constant coefficients,

$$(\mathscr{D}^2 - \alpha^2 - \beta^2)^2\tilde{v} - \mathrm{i}Re_{\delta^*}(\alpha U_\infty + \beta W_\infty - \omega)\,(\mathscr{D}^2 - \alpha^2 - \beta^2)\tilde{v} = 0, \tag{2.13a}$$

$$(\mathscr{D}^2 - \alpha^2 - \beta^2)\tilde{\eta} - \mathrm{i}Re_{\delta^*}(\alpha U_\infty + \beta W_\infty - \omega)\,\tilde{\eta} = 0. \tag{2.13b}$$

$\tilde{v}$ and $\tilde{\eta}$ are the amplitude functions in spectral space for the normal velocity v and vorticity η of the continuous Orr–Sommerfeld/Squire eigenmodes, α is the chordwise wavenumber and $\mathscr{D} = \mathrm{d}/\mathrm{d}y$. Defining

$$\gamma^2 \equiv -\mathrm{i}Re_{\delta^*}(\alpha U_\infty + \beta W_\infty - \omega) - \alpha^2 - \beta^2, \tag{2.14}$$

(2.13) can be re-written as

$$(\mathscr{D}^2 - \alpha^2 - \beta^2)(\mathscr{D}^2 + \gamma^2)\tilde{v} = 0, \tag{2.15a}$$

$$(\mathscr{D}^2 + \gamma^2)\tilde{\eta} = 0. \tag{2.15b}$$

Further, (2.14) can be re-ordered to obtain a quadratic equation in α with solution

$$\alpha = \frac{1}{2}\mathrm{i}[\sqrt{(Re_{\delta^*}U_\infty)^2 + 4(\mathrm{i}Re_{\delta^*}(\beta W_\infty - \omega) + \beta^2 + \gamma^2)} - Re_{\delta^*}U_\infty], \tag{2.16}$$

which is the dispersion relation for the continuous Orr–Sommerfeld/Squire eigenmodes. The term $(\mathscr{D}^2 + \gamma^2)$ in (2.15) suggests the interpretation of γ as a wall-normal wavenumber. The solution to (2.15) is,

$$\tilde{v} = A\mathrm{e}^{-\mathrm{i}\gamma y} + B\mathrm{e}^{\mathrm{i}\gamma y} + C\mathrm{e}^{-\sqrt{\alpha^2+\beta^2}y} + D\mathrm{e}^{\sqrt{\alpha^2+\beta^2}y}, \tag{2.17a}$$

$$\tilde{\eta} = E\mathrm{e}^{-\mathrm{i}\gamma y} + F\mathrm{e}^{\mathrm{i}\gamma y}. \tag{2.17b}$$

The constants A to F result from the boundary conditions on the plate and in the outer flow. To avoid a non-physical 'exploding' solution as $y \to \infty$, the fourth fundamental solution for $\tilde{v}$ should be dropped. In practice, to compute the free-stream modes, the upper boundary is located a sufficiently large wall-normal distance y_∞ away from the plate. There, we may impose arbitrary normalization conditions $\tilde{v}_\infty$ and $\tilde{\eta}_\infty$. The boundary conditions for $\tilde{v}$ and $\tilde{\eta}$ at the wall and in the free stream are then

$$y = 0: \qquad \tilde{v} = \mathscr{D}\tilde{v} = \tilde{\eta} = 0, \tag{2.18a}$$

$$y = y_\infty: \qquad \tilde{v} = \tilde{v}_\infty,\ \tilde{\eta} = \tilde{\eta}_\infty. \tag{2.18b}$$

These five conditions determine the constants in (2.17), and a shooting method can be employed to solve (2.13). Jacobs & Durbin (1998) observe, however, that shooting techniques often do not converge, in particular when ω is small. They suggest instead a method to impose a boundedness condition for the eigenfunction $\tilde{v}$ at y_∞, based on the evaluation of $(\mathscr{D}^2 + \gamma^2)\tilde{v}$ at two points y_1 and y_2 in the free stream,

$$\frac{\left[(\mathscr{D}^2 + \gamma^2)\tilde{v}\right]_{y_1}}{\left[(\mathscr{D}^2 + \gamma^2)\tilde{v}\right]_{y_2}} = \mathrm{e}^{\sqrt{\alpha^2+\beta^2}(y_2-y_1)}. \tag{2.19}$$

This amounts to a boundary-value problem for $\tilde{v}$ with the conditions (2.18a) at the wall and condition (2.19) near the free-stream boundary. The normalization

https://doi.org/10.1017/S0022112008004345 Published online by Cambridge University Press

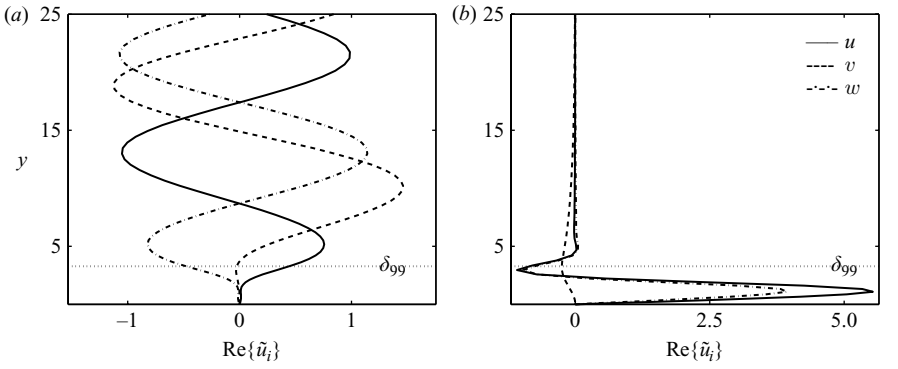


FIGURE 3. (*a*) Wall-normal shape of a free-stream eigenmode from the continuous spectrum of the Orr–Sommerfeld equation, $(\alpha, \beta) = (0.130, -0.140)$, $\alpha_i = 0.00081$, $\gamma = 0.377$, $\omega = -0.01$. (*b*) Amplitude in the wall-normal direction of a travelling discrete boundary-layer eigenmode, $(\alpha, \beta) = (0.102, -0.140)$, $\alpha_i = 0.00474$, $\omega = -0.01$.

(2.18*b*) is then used to scale the mode to the desired energy. In summary, the spatial eigenvalue α is obtained from (2.16), and the associated eigenfunctions for $\tilde{v}$ and $\tilde{\eta}$ from the numerical solution of the Orr–Sommerfeld/Squire system together with the boundary conditions (2.18) and (2.19). The chordwise and spanwise spectral velocities $\tilde{u}$ and $\tilde{w}$ are computed from the definition of $\tilde{\eta}$ in conjunction with the continuity equation. The shape of a continuous eigenmode along the wall-normal coordinate y is shown in figure 3(*a*). Clearly, the amplitude of the eigenfunction is quenched to zero towards the plate, as desired, and oscillates in the free stream. Therefore, the continuous modes are herein also referred to as free-stream modes. Figure 3(*b*) shows the wall-normal amplitude for an eigenmode from the discrete spectrum of the Orr–Sommerfeld/Squire operator. Since it is large inside the boundary layer and tends to zero in the outer flow, the discrete modes are often called boundary-layer modes. In contrast to the free-stream modes, which are always damped, there exist unstable discrete modes in three-dimensional boundary layers for certain parameter combinations $(m, \phi_0; Re_{\delta^*}, \beta, \omega)$, where β and ω are the spanwise wavenumber and the angular frequency of the eigenmode. The crossflow instability waves are an example for unstable discrete modes, and figure 3(*b*) shows a crossflow mode.

As already mentioned, the vortical free-stream mode is imposed in the fringe region and re-cycled to the inflow plane of the computational domain. Therefore, when computing the continuous mode, the Reynolds number is fixed to the inflow value $Re_{\delta_0^*}$, whereas β, γ and ω can be chosen arbitrarily. In § 4, the choice of the continuous-spectrum eigenmodes as a model for free-stream disturbances will be motivated.

To study the spatial evolution of the unstable modes, we may superimpose a discrete boundary-layer mode on the base flow in the same manner as the continuous free-stream mode. The spatial eigenvalues and eigenshapes of the discrete modes are computed by solving the spatial Orr–Sommerfeld/Squire eigenvalue problem, as described in Schmid & Henningson (2001), for instance.

2.4. *Computational domain and numerical resolution*

Table 1 gives the dimensions L_x, L_y and L_z of the computational domain together with the corresponding resolution N_x, N_y and N_z along the spatial coordinates. The range of inflow Reynolds numbers $Re_{\delta_0^*}$ and the type of disturbance forcing are also

https://doi.org/10.1017/S0022112008004345 Published online by Cambridge University Press

Box	$L_x \times L_y$	L_z	$N_x \times N_y \times N_z$	$Re_{\delta_0^*}$	Disturbance forcing
A	883.2×20.0	$12.0 \ldots 73.0$	$768 \times 65 \times 8$	220	Surface roughness
B	2048.0×50.0	$23.0 \ldots 73.0$	$512 \times 97 \times 4$	$220 \ldots 353$	Free-stream mode
C	3072.0×50.0	33.0, 66.0, 99.0	$1536 \times 97 \times 12$	220	Surface roughness + free-stream mode

TABLE 1. Dimensions and resolution of the computational domain. Inflow Reynolds number and type of disturbance forcing.

given in the table. Three different computational boxes, A, B and C, have been used to obtain the results for receptivity to wall roughness, vortical free-stream modes and their combination. Note that the spanwise width L_z of the domain has been varied for boxes A and B to study the receptivity when varying the spanwise wavenumber of the unstable waves, and that the inflow Reynolds number $Re_{\delta_0^*}$ has been also varied when studying the effect of free-stream modes. The box dimensions L_x, L_y, and L_z have been scaled in such a way that the physical box dimensions $L_x\delta_0^*$, $L_y\delta_0^*$, and $L_z\delta_0^*$, and thus the resolution, remain unchanged for all values of $Re_{\delta_0^*}$. The listed values of L_x, L_y and L_z for box B refer to $Re_{\delta_0^*} = 220$.

3. Receptivity of stationary modes to localized wall roughness

It is known that surface roughness provides an efficient mechanism for the excitation of steady crossflow instability waves if the roughness contour contains the wavenumber of the instability (see e.g. Crouch 1993; Choudhari 1994; Bertolotti 2000). The receptivity process, connecting the forcing due to the roughness element with the response of the boundary layer, is described in terms of the receptivity coefficient $C_R(\beta_R, \omega; m, \phi_0)$, where β_R is the spanwise wavenumber of the roughness, and the frequency ω is zero for steady surface roughness,

$$C_R = \frac{A_R}{\varepsilon_h H(\alpha_{CF})}. \tag{3.1}$$

A_R is the receptivity amplitude, i.e. the amplitude of the excited steady crossflow instability at the roughness station x_R, defined at the centre of the bump. $H(\alpha_R)$ denotes the representation of the chordwise bump shape $h_x(x)$ in Fourier space, and α_{CF} is the chordwise wavenumber of the excited stationary crossflow instability at x_R. Here, the wall-normal maximum of $\sqrt{\overline{u^2}}$ is chosen as the measure for the boundary-layer response, where u is the chordwise disturbance velocity. C_R may be interpreted as the efficiency of the forcing mechanism – here the roughness bump – in exciting the least stable eigenmode of the boundary layer – here the steady crossflow mode. A similar definition is used in Crouch (1993), Choudhari (1994) and Ng & Crouch (1999) in the context of finite Reynolds-number theory. In contrast to these studies, non-parallel effects on the receptivity process are included here by employing direct numerical simulation. Various roughness elements are considered, differing in their chordwise shape $h_x(x)$ as well as in their spanwise wavenumber β_R. Most of the results are obtained by using roughness with maximum amplitude ε_h being much smaller than the characteristic length δ_0^* of the basic flow such that the linearized perturbation equations are valid. In § 3.2 higher roughness elements are also considered and the nonlinear disturbance equations are solved. Three chordwise roughness contours are considered, with parameters compiled in table 2. In order to

https://doi.org/10.1017/S0022112008004345 Published online by Cambridge University Press

Shape	ε_h	h_{start}	h_{end}	h_{rise}	h_{fall}
I	0.021	4.6	32.2	11.5	11.5
II	0.021	9.2	27.6	6.9	6.9
III	0.021	13.8	23.0	3.45	3.45

TABLE 2. Three different chordwise shape functions $h_x(x)$ for surface roughness. Parameters according to (2.9) and (2.10).

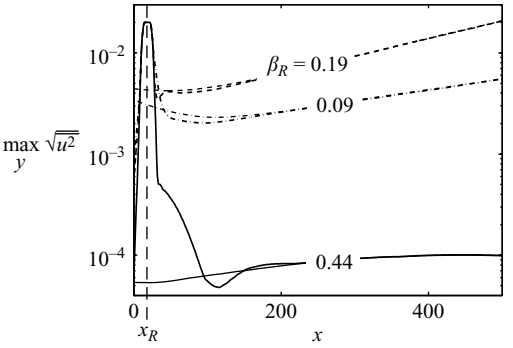


FIGURE 4. Boundary-layer response to roughness at $x_R = 18.4$ ($Re_{\delta^*} = 234$), expressed as wall-normal maximum of the chordwise disturbance-velocity amplitude (thick lines), and evolution of the excited steady crossflow instability waves (thin lines).

investigate the dependence of the receptivity coefficient C_R on the spanwise scale of the roughness, the width L_z of the domain is changed according to table 1. The values for box A correspond to spanwise roughness wavenumbers β_R between 0.09 and 0.52.

3.1. *Low-amplitude roughness*

Figure 4 shows the boundary-layer response to perturbations caused by roughness elements of different spanwise wavenumbers β_R (thick lines). For each case, a second simulation employing a smooth plate is performed, where the wall-normal velocity distribution of the stationary crossflow eigenmode at $|\beta_{CF}| = \beta_R$ is prescribed at the inflow plane. The response of the base flow to this initial condition is displayed as a thin line in figure 4. Comparison of the thick and the thin curves reveals that the flow response in the vicinity of the roughness is characterized by transient behaviour, while the downstream evolution of the boundary-layer disturbance is fully determined by the excited steady crossflow instability. The receptivity amplitude A_R is extracted from the total disturbance (thick lines) by tracing back the contribution of the unstable crossflow mode (thin lines) to the roughness station x_R. It can be concluded that surface roughness provides an efficient linear mechanism for the excitation of zero-frequency crossflow instability.

Figure 4 also suggests that the efficiency of the receptivity mechanism is strongly dependent on the spanwise wavenumber of the roughness element. Further, to verify the assumption of shape-independent receptivity, roughness elements of different chordwise shape are considered. These two aspects have been investigated in detail, and the result is reported in figure 5. In figure 5(*a*), the three chordwise roughness contours under consideration are displayed in physical (insertion) and in Fourier space. Depending on their spanwise wavenumber β_R, these roughness elements will force

https://doi.org/10.1017/S0022112008004345 Published online by Cambridge University Press

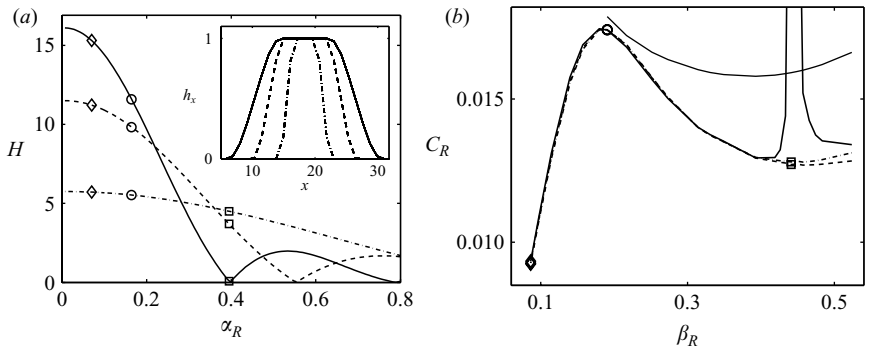


FIGURE 5. (*a*) Three roughness shapes in physical (inset) and spectral space. The symbols mark the Fourier component of the spectral bump shape at the chordwise wavenumber α_{CF} of the excited steady crossflow eigenmode (i.e. $\alpha_{CF} = \alpha_R$), shown for three spanwise wavenumbers of the roughness: $\beta_R = 0.09$ (◇), 0.19 (○) and 0.44 (□). (*b*) Thick lines: receptivity coefficient in spatially evolving flow versus spanwise wavenumber of the roughness for the three bump shapes in (*a*). The roughness is placed at $x_R = 18.4$ ($Re_{\delta^*} = 234$). The symbols correspond to those in (*a*). Thin solid line: receptivity coefficient in parallel flow.

different unstable boundary-layer modes with different efficiency. This is highlighted in the figure by the symbols, marking the spectral component $H(\alpha_{CF})$ for different roughness elements. $H(\alpha_{CF})$ measures to which degree the chordwise wavenumber α_{CF} of the triggered stationary crossflow mode is represented in the three spectral shape functions. In figure 5(*b*), the influence of chordwise shape and spanwise wavenumber of the roughness on the receptivity coefficient is depicted. Results for receptivity in parallel boundary layers are also included (thin curve). They are obtained by employing the same roughness elements in parallel base flow for the Reynolds number at the roughness station, i.e. $Re_{\delta^*} = 234$. The receptivity coefficients C_R in parallel flow could be extracted solely for wavenumbers pertaining to unstable or marginally stable crossflow modes. In these cases, the least stable mode is clearly distinguishable from the total disturbance further downstream. It can be concluded from figure 5(*b*) that non-parallel flow (thick lines) is less receptive to roughness-induced perturbations than parallel flow (thin line). In particular, roughness elements of large spanwise wavenumber, triggering instabilities with short wavelengths, give lower receptivity coefficients in spatially developing flow. This is in line with the findings of Collis & Lele (1999) who demonstrated that non-parallel effects attenuate roughness-related receptivity. They used the steady solution to flow around a swept parabolic cylinder as base flow and applied a bump of Gaussian shape near the leading edge.

Two additional conclusions can be drawn from figure 5(*b*). (i) An optimal spanwise wavenumber, $\beta_R \approx 0.19$, can be identified, at which the receptivity process in non-parallel flow is most efficient. (ii) For the three roughness contours under consideration, the receptivity coefficient is independent of the specific shape over a large range of values for β_R. However, for $\beta_R \gtrsim 0.41$, the shape-independence of C_R is broken. For roughness contour I (solid line), the C_R curve exhibits a remarkable jump around $\beta_R = 0.44$. Comparing figures 5(*a*) and 5(*b*) reveals that this jump is occurring, as bump shape I has almost zero component $H(\alpha_{CF})$ at the instability wavenumber $(\alpha_{CF}, |\beta_{CF}|) = (0.40, 0.44)$ (square symbol). Also, the amplitude A_R of the unstable eigenmode is small, if $\beta_R = 0.44$, as shown in figure 4. The receptivity coefficient C_R no longer provides a shape-independent universal measure for receptivity to roughness, if both numerator and denominator in (3.1) become small. In such situations, C_R

https://doi.org/10.1017/S0022112008004345 Published online by Cambridge University Press

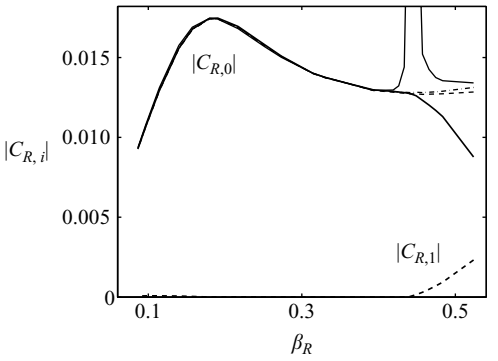


FIGURE 6. Thick lines: receptivity coefficients $|C_{R,0}|$ (——) and $|C_{R,1}|$ (---) according to (3.2). Thin lines: receptivity coefficient C_R, (3.1), as in figure 5(*b*).

describes the receptivity process improperly; moreover, C_R is no longer well-defined, when $H(\alpha_{CF})$ is zero. Also, the receptivity coefficients computed from the roughness contours II and III start to differ for large values of β_R, i.e. when the bump is longer than the crossflow wavelength.

Unlike in parallel flow, where the receptivity amplitude A_R of the crossflow mode vanishes as $H(\alpha_{CF}) \to 0$, low values of A_R are still observed in downstream-evolving boundary layers, even when the spectrum of the roughness element contains no energy at all at the instability wavenumber. The receptivity coefficient C_R, derived for parallel base flow, cannot capture this non-parallel effect. To provide an improved measure for roughness-related receptivity when $H(\alpha_{CF})$ becomes small, Bertolotti (2000) suggests an alternative expression for the receptivity amplitude,

$$A_R = \varepsilon_h |C_{R,0} H(\alpha_{CF}) + C_{R,1} H'(\alpha_{CF})|, \tag{3.2}$$

i.e. a second term depending on the slope $H'(\alpha_{CF}) \equiv (\mathrm{d}H/\mathrm{d}\alpha)_{\alpha_{CF}}$ is introduced. Bertolotti derives (3.2) by expanding the base flow and the disturbance in the chordwise direction about the roughness station x_R. The expansion is truncated at first order and analysed in spectral space. As shown in Bertolotti (2000), the term $C_{R,0} H(\alpha_{CF})$ represents the contribution to A_R at zeroth order, while $C_{R,1} H'(\alpha_{CF})$ is the first-order correction due to the non-parallel evolution of the base flow.

The zeroth- and first-order receptivity coefficients $C_{R,0}$ and $C_{R,1}$ can be extracted from the present DNS data by solving the following linear system,

$$\begin{pmatrix} C_{R,0} \\ C_{R,1} \end{pmatrix} = \frac{1}{\varepsilon_h} \begin{pmatrix} H_1 & H_1' \\ H_2 & H_2' \end{pmatrix}^{-1}_{\alpha_{CF}} \begin{pmatrix} A_{R,1} \\ A_{R,2} \end{pmatrix}_{DNS}, \tag{3.3}$$

using two of the roughness contours under consideration. The validity of Bertolotti's ansatz for A_R is checked by applying (3.2) with the coefficients $C_{R,0}$ and $C_{R,1}$ from (3.3) to results obtained when forcing with the third roughness contour,

$$A_{R,3}|_{pred} = \varepsilon_h (C_{R,0} H_3 + C_{R,1} H_3')_{\alpha_{CF}} \equiv A_{R,3}|_{DNS}. \tag{3.4}$$

$A_{R,3}|_{pred}$ denotes the wave amplitude and phase predicted by model (3.2), and $A_{R,3}|_{DNS}$ is the receptivity amplitude obtained by DNS. $A_{R,3}|_{pred} = A_{R,3}|_{DNS}$ is indeed obtained with good accuracy for all spanwise wavenumbers under consideration, both in terms of amplitude and phase. The receptivity coefficients $|C_{R,0}|$ and $|C_{R,1}|$ are plotted versus β_R in figure 6. Clearly, there is very good agreement between the standard receptivity coefficient C_R and the zeroth-order coefficient $|C_{R,0}|$ for $\beta_R \lesssim 0.41$. In this regime,

https://doi.org/10.1017/S0022112008004345 Published online by Cambridge University Press

receptivity to roughness is adequately described by a receptivity coefficient based only on $H(\alpha_{CF})$. For $\beta_R \gtrsim 0.41$, however, the correction term $C_{R,1}H'(\alpha_{CF})$ is no longer negligible. $|C_{R,0}|$ drops down in this region and no longer exhibits the peak seen in the curve for C_R. $|C_{R,0}|$ in combination with $|C_{R,1}|$ is thus a more appropriate measure for receptivity to roughness bumps with very low spectral amplitude $H(\alpha_{CF})$ than the standard coefficient C_R. Following Bertolotti (2000) who attributes the contribution proportional to $H'(\alpha_{CF})$ to the non-parallel nature of the base flow, we conclude from figure 6 that the non-parallel correction $C_{R,1}H'(\alpha_{CF})$ is most important for large wavenumbers of the triggered unstable boundary-layer mode. The wavelength of the crossflow disturbance is then considerably shorter than the chordwise extent of the roughness element. Since $|C_{R,0}|$ and $|C_{R,1}|$ fulfil (3.2) for all three roughness contours, they represent to first order a shape-independent universal measure for receptivity to roughness. To summarize, the non-parallel nature of the base flow becomes manifest in two ways: a stronger effect over the whole wavenumber range plotted in figure 5(*b*) and a weaker effect only for large wavenumbers displayed in figure 6.

A roughness element with even larger chordwise length may be designed such that the spectral shape has a zero crossing at $(\alpha_{CF}, \beta_{CF}) = (0.17, -0.19)$, that is, at the most receptive wavenumber. We have performed a simulation with a bump with $H(\alpha_{CF} = 0.17) = 9.6 \times 10^{-2}$, which is about 60 times smaller than the spectral amplitude of the short bump contour III at that wavenumber. The difference in amplitude A_R of the triggered unstable mode is, however, much less; A_R is 9.6×10^{-4} for the long versus 1.7×10^{-3} for the short roughness element. The curve for the classical receptivity coefficient C_R would again exhibit large peaks at every zero crossing of the spectral contour H, while the curves for $|C_{R,0}|$ and $|C_{R,1}|$ look smooth. They differ, however, from the corresponding curves in figure 6 in that the contribution of the first-order coefficient $|C_{R,1}|$ becomes stronger. We conclude that the receptivity coefficients $|C_{R,0}|$ and $|C_{R,1}|$ preserve their independence of roughness shape only within a limited range of bump length. For longer, less localized roughness elements, contributions related to higher derivatives of H are likely to come into play. We want to emphasize, however, that the classical receptivity coefficient C_R is nevertheless an appropriate representation of roughness receptivity in the framework of localized receptivity.

The response of the base flow to disturbances introduced by localized roughness elements at different chordwise stations x_R is studied next. Bump shape III is considered here. The spanwise scale of the roughness is chosen to be $\lambda_z = 50$ inflow displacement thicknesses, corresponding to $\beta_R = 0.126$. These values match approximatively the spanwise scale of the roughness array in the experiments by Reibert *et al.* (1996). As shown in the previous section, the standard receptivity coefficient C_R is independent of the roughness shape at $\beta_R = 0.126$ and can thus be used here. The dependence of C_R on the chordwise position x_R of the roughness element is depicted in figure 7 (solid line). The dashed line shows the effective receptivity coefficient $C_{R,eff}$, compensating for the local decay or growth of the excited steady crossflow instability at x_R,

$$C_{R,eff} = \frac{C_R}{\mathrm{e}^{N_R}} = C_R \frac{A_I}{A_R} = \frac{A_I}{\varepsilon_h H(\alpha_{CF})}, \tag{3.5}$$

where N_R is the N-factor of the crossflow disturbance at x_R, and A_I is the amplitude at the first neutral point of the crossflow mode. While C_R is a measure for the receptivity process only, $C_{R,eff}$ can be used to determine the disturbance amplitude $A(x)$ in the

https://doi.org/10.1017/S0022112008004345 Published online by Cambridge University Press

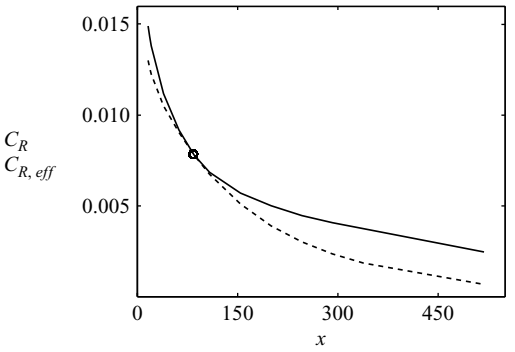


FIGURE 7. Receptivity coefficient for surface roughness as a function of the chordwise station x_R of the roughness element (——). Roughness shape III is used, and $\beta_R = 0.126$. Effective receptivity coefficient $C_{R,eff}$ (---). ○, first neutral point of the excited steady cross-flow mode.

linear regime downstream of the roughness,

$$A(x) = \varepsilon_h H(\alpha_{CF}) C_{R,eff} \mathrm{e}^{N(x)}. \tag{3.6}$$

The receptivity process is most efficient upstream of the first neutral point and drops down rapidly downstream of it. This is in line with results for parallel flow, obtained by finite Reynolds-number theory (see e.g. Crouch 1993).

3.2. *Larger-amplitude roughness*

In the previous section, receptivity to localized surface roughness of low amplitude was discussed. The amplitude A_R of the excited unstable crossflow mode is then proportional to the height ε_h of these tiny roughness elements, leading to constant receptivity coefficients as ε_h is changed. In this section, receptivity to roughness with higher amplitude is investigated to identify at which bump height nonlinear behaviour starts to affect the receptivity. The roughness elements used here are of shape I, II and III and have a fixed spanwise wavenumber of $\beta_R = 0.19$. This choice guarantees efficient receptivity and negligible non-parallel effects, as seen before. The height of the roughness elements is chosen in the range $0.02 \leqslant \varepsilon \leqslant 0.2$. At the highest bump amplitude $\varepsilon = 0.2$, a region of linear growth of the unstable mode is no longer clearly identified, whereas the flow downstream of the roughness is characterized by saturating crossflow modes. Nonlinear behaviour is hence apparent at this roughness amplitude. However, also below this height, nonlinearity has an effect on receptivity figure (8). Beyond $\varepsilon = 0.05$, C_R becomes dependent on both the amplitude and the shape of the roughness element. In particular, the dashed-dotted curve obtained by inserting the shortest roughness element (shape III) deviates to lower values from the constant C_R found for low roughness height. Bump I, conversely, retains a constant receptivity efficiency even for nonlinearly behaving crossflow modes. In summary, the deviation of C_R from its value for tiny roughness remains rather small for the plotted range of roughness amplitudes, i.e. nonlinearity has a weaker effect on the receptivity process than on the subsequent growth of the triggered instability (saturation).

4. Receptivity of travelling crossflow modes to vortical free-stream disturbances

In this section, we investigate whether three-dimensional boundary-layer flow over a smooth plate is receptive to vortical free-stream perturbations. The disturbance is

https://doi.org/10.1017/S0022112008004345 Published online by Cambridge University Press

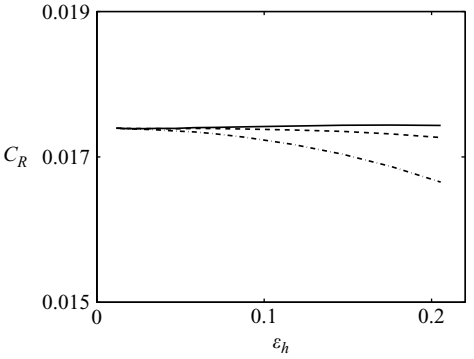


FIGURE 8. Effect of bump height on receptivity to surface roughness. $\beta_R = 0.19$. Bump shape I (——), II (---) and III (-·-).

modelled by means of eigenfunctions from the continuous wavenumber spectrum of the Orr–Sommerfeld/Squire operator, which are often called continuous modes. Since free-stream turbulence is in general an unsteady phenomenon, the study is restricted to the unsteady receptivity process. In particular, receptivity to one single free-stream mode is examined, nonlinear interaction with other modes being neglected. The computation of the Orr–Sommerfeld solution $\tilde{v}$ and the Squire solution $\tilde{\eta}$ in the free stream has been outlined in § 2.3.2. The chordwise and spanwise disturbance velocities $\tilde{u}$ and $\tilde{w}$ can be calculated from the normal velocity $\tilde{v}$ and vorticity $\tilde{\eta}$ as

$$\tilde{u} = \tilde{u}_{OS} + \tilde{u}_{Sq} = \frac{\mathrm{i}\alpha}{\alpha^2+\beta^2}\mathscr{D}\tilde{v} - \frac{\mathrm{i}\beta}{\alpha^2+\beta^2}\tilde{\eta}, \tag{4.1a}$$

$$\tilde{w} = \tilde{w}_{OS} + \tilde{w}_{Sq} = \frac{\mathrm{i}\beta}{\alpha^2+\beta^2}\mathscr{D}\tilde{v} + \frac{\mathrm{i}\alpha}{\alpha^2+\beta^2}\tilde{\eta}. \tag{4.1b}$$

The Orr–Sommerfeld and the Squire solution are hence coupled in the $\tilde{u}$ and the $\tilde{w}$ component of the eigenmode $(\tilde{u}, \tilde{v}, \tilde{w}, \tilde{\eta})^T$. Instead of such a full continuous-spectrum mode, a continuous mode without the $\tilde{\eta}$ contribution can be considered, i.e. $(\tilde{u}_{OS}, \tilde{v}, \tilde{w}_{OS}, 0)^T$. As only the contribution of the Orr–Sommerfeld equation is present in such a mode, it is referred to as the Orr–Sommerfeld mode here. The use of Orr–Sommerfeld modes as a model for free-stream vorticity can be justified as follows. In the flow upstream of the leading edge of the plate there is no coupling between normal velocity and vorticity. Homogeneous isotropic turbulence is an example of an incoming flow with independent evolution of $\tilde{v}$ and $\tilde{\eta}$. The coupling sets in, when the flow attaches to the plate at the leading edge. The Orr–Sommerfeld mode forces the corresponding set of Squire modes and develops gradually into a full mode. This is a viscous slow process. In the simulations, the free-stream mode is introduced a short distance downstream of the leading edge, where the forcing of the Squire modes and thus the coupling between $\tilde{v}$ and $\tilde{\eta}$ has just been initiated. For the cases considered here, the shape of the free-stream disturbance is still similar to that of the Orr–Sommerfeld mode without the $\tilde{\eta}$ contribution.

4.1. *Penetration depth and chordwise decay*

Two different characteristics of the Orr–Sommerfeld free-stream modes have been identified to play a role for unsteady receptivity: their ability to penetrate into the boundary layer and their downstream decay rate. Jacobs & Durbin (1998) introduce

https://doi.org/10.1017/S0022112008004345 Published online by Cambridge University Press

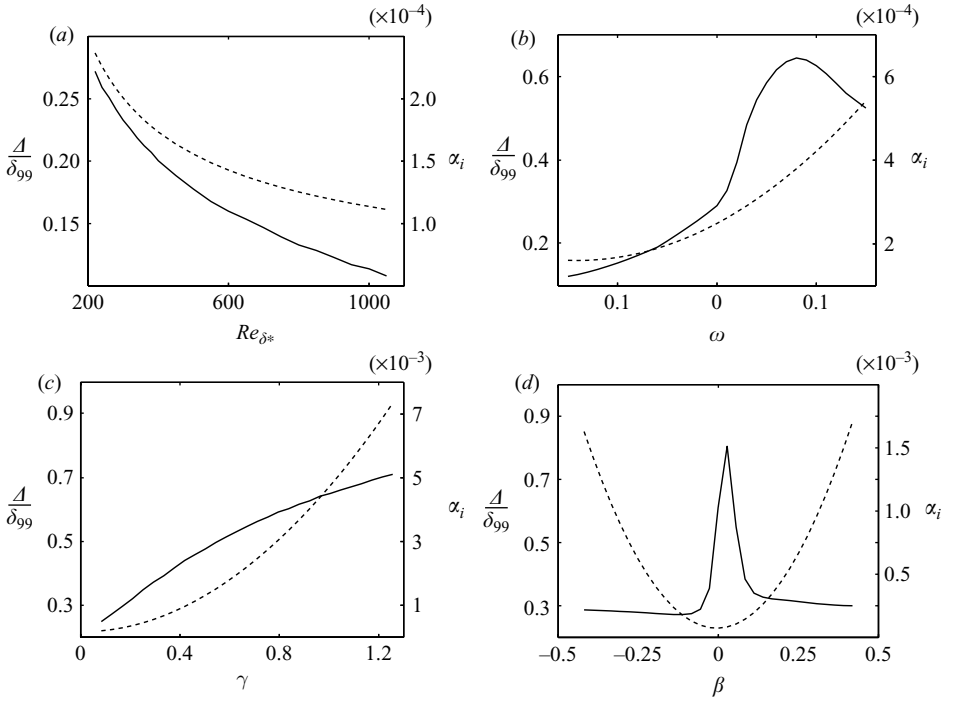


FIGURE 9. Penetration depth Δ (——) and decay rate α_i (---) of the continuous Orr–Sommerfeld modes for ranges of (*a*) Reynolds number Re_δ, (*b*) angular frequency ω, (*c*) wall-normal wavenumber γ and (*d*) spanwise wavenumber β. The plots are based on $(Re_\delta, \omega; \beta, \gamma) = (220, -0.01; -0.14, 0.126)$.

the penetration depth Δ as the distance from the boundary-layer edge, at which the magnitude of the eigenshape $\tilde{v}$ has decayed to 1 % of its free-stream value. They obtained a relationship for Blasius flow between Δ, frequency ω and Reynolds number $Re = \sqrt{U_\infty^* x^*/\nu^*}$,

$$\Delta \sim (\omega Re)^{-b}, \tag{4.2}$$

where the exponent b takes values of the order of 0.1 depending on the wall-normal wavenumber γ. Zaki & Durbin (2005) point out that not only the penetration depth, but also the decay rate of the vortical disturbance must be considered. The free-stream mode is efficient in perturbing the boundary layer if it penetrates deeply into it, or if it decays slowly and thus carries enough energy downstream. At fixed Re and ω, these two features are competitive: deeply penetrating modes with large γ decay rapidly, while modes with smaller γ penetrate and decay less. Maslowe & Spiteri (2001) present a similar analysis for the continuous-spectrum modes of a two-dimensional boundary layer in a streamwise pressure gradient modelled by the Falkner–Skan similarity solution. They find that (4.2) holds also for the adverse pressure-gradient boundary layer. However, the constant of proportionality is different, as shown in Zaki & Durbin (2006): Penetration depth is reduced in adverse and enhanced in favourable pressure gradient as compared to Blasius flow.

We perform a similar investigation of penetration depth and decay rate of the continuous-spectrum modes in the three-dimensional boundary layer. A parametric study for free-stream modes in Falkner–Skan–Cooke flow is presented in figure 9.

https://doi.org/10.1017/S0022112008004345 Published online by Cambridge University Press

The behaviour of the penetration depth Δ (solid) and decay rate α_i (dashed) of the continuous Orr–Sommerfeld modes is shown for ranges of (*a*) Reynolds number, (*b*) angular frequency, (*c*) wall-normal wavenumber and (*d*) spanwise wavenumber. Δ is normalized by the 99 % boundary-layer thickness and is defined as the distance below the boundary-layer edge, at which the chordwise disturbance amplitude $|\tilde{u}|$ has dropped to 5 % of its maximum value in the outer flow. Figures 9(*a*) to 9(*c*) reveal that deeply penetrating free-stream modes suffer from a strong decay. In figure 9(*a*), a large penetration depth of more than 25 % of the boundary-layer thickness is obtained at small Reynolds numbers, i.e. close to the leading edge of the plate, whereas Δ quickly drops downstream.

The penetration depth assumes large values in the positive ω half-plane in figure 9(*b*) and the maximum is obtained at $\omega = 0.08$. This is in contrast to the result for Blasius flow, (4.2), where Δ approaches its maximum for $\omega \to 0$. The most unstable crossflow modes are, however, obtained for $\omega < 0$, i.e. the negative frequency range is more relevant for the study of receptivity to continuous modes. Note that the counterpart of ω in the dispersion relation for Blasius flow is the quantity $(\omega - \beta W_\infty)$ in (2.16) here, which is positive in figure 9(*b*) also in the range of negative ω. We could not find a relation for the penetration depth Δ corresponding to (4.2), either in terms of ωRe or of $(\omega - \beta W_\infty)Re$. In light of the observation by Maslowe & Spiteri (2001) that the free-stream modes in Falkner–Skan flow behave similarly to those in Blasius flow, it can be concluded that the different behaviour of Δ with ω, β and Re is a result of the spanwise component of the base flow.

As shown in figure 9(*c*), penetration depth grows with increasing wall-normal wavenumber. The free-stream modes of the smallest normal length scale penetrate the boundary layer to a depth of up to 70 % of its thickness, although they die out rapidly.

In figure 9(*d*), a region of deep penetration exists, while the decay rate is small. The curve for Δ exhibits a remarkable peak at small spanwise wavenumbers. These waves have also a small chordwise wavenumber. At $\beta = 0$, the continuous mode becomes a two-dimensional wave. The most deeply penetrating free-stream modes are thus long waves propagating nearly perpendicularly to the leading edge. However, these modes are irrelevant for the present receptivity study, since they do not trigger boundary-layer instabilities. The most unstable travelling eigenmodes are found at negative values of β, while $\alpha > 0$. These disturbances propagate in the direction of the crossflow. In this wavenumber regime, the penetration depth for free-stream vorticity is almost constant at a level of $\simeq 28$ %.

To conclude, comparison with the results in Jacobs & Durbin (1998) reveals that in Falkner–Skan–Cooke flow, mean shear hampers the penetration of free-stream vorticity into the boundary layer much more than in Blasius flow.

4.2. *Scale conversion*

Direct excitation of travelling boundary-layer instability waves requires an external perturbation with matching wavenumber vector and frequency. Free-stream disturbances, however, have, in general, different length scales to the unstable eigenmode of the boundary layer. Goldstein (1985) demonstrates for Blasius flow that there is nonetheless a receptivity mechanism to acoustic free-stream disturbances, triggering Tollmien–Schlichting (TS) instability. He introduces the concept of scale reduction, by which the large length scale of the acoustic wave is converted into the smaller scale of the TS wave. Goldstein (1985) shows that the scale-conversion process is efficient, in particular around a surface irregularity. Scattering of acoustic

https://doi.org/10.1017/S0022112008004345 Published online by Cambridge University Press

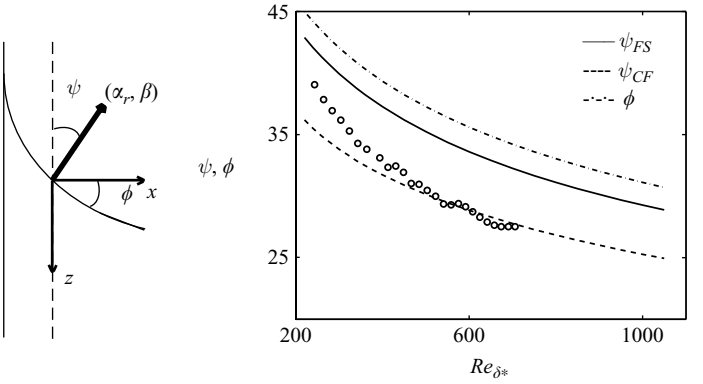


FIGURE 10. Horizontal wavenumber angle $\psi = \arctan(\alpha_r/|\beta|)$ for the continuous Orr–Sommerfeld mode ($\omega = -0.01$, $\beta = -0.14$, $\gamma = 0.126$, ——) and the excited travelling crossflow wave (---) and local angle ϕ of the external streamline (---). The symbols mark the wave angle of the forced boundary-layer disturbance and are extracted from DNS data.

waves at roughness elements, suction holes or other types of wall disturbances has indeed been shown to be an efficient receptivity mechanism for TS waves (e.g. Crouch 1992; Choudhari & Streett 1992; Crouch & Spalart 1995).

Also, in swept-plate flow, the horizontal length scales of the free-stream perturbations differ from those of the boundary-layer disturbances. In figure 10, the angle $\psi = \arctan(\alpha_r/|\beta|)$ of the horizontal wavenumber vector of a vortical free-stream mode and a travelling crossflow mode are compared. Both modes are computed at a frequency of $\omega = -0.01$ and a spanwise wavenumber of $\beta = -0.14$. The angle of the outer streamline is also plotted for comparison, showing that the free-stream vortex is more closely aligned with the external streamlines than the unsteady crossflow wave. Clearly, the wavenumber vectors for the free-stream wave and the crossflow mode are not aligned at any location, which reflects their different chordwise wavenumber $\alpha_r = \mathrm{Re}\{\alpha\}$. Specifically, the chordwise wavenumber of the travelling crossflow mode is smaller than that of the free-stream disturbance. Further, the relative misalignment between the two waves is nearly constant versus Re_{δ^*}. Therefore there is no direct resonance between the vortical free-stream disturbance and the unsteady crossflow instability at any location in the flow, and it can be concluded that length-scale conversion will be a key element for unsteady receptivity also in three-dimensional boundary layers. This becomes evident in figure 10 by the symbols showing the wave-vector angle of the largest fluctuations inside the boundary layer, when it is forced by a vortical free-stream mode. These data have been extracted from a DNS velocity field. Upstream, the wave vector of the forced disturbance is more closely aligned with the free-stream mode, whereas it turns into the direction of the excited crossflow mode further downstream. It also becomes apparent that in contrast to Blasius flow, the chordwise length scale of the free-stream disturbance must be enhanced rather than reduced to match that of the boundary-layer eigenmode. Since scale conversion relies on rapid mean-flow changes, it is expected to be efficient in particular in the strongly developing upstream region of the boundary layer and around wall roughness.

4.3. *Receptivity coefficient*

Receptivity of the Blasius boundary layer to vortical disturbances in the outer flow has been thoroughly investigated previously. Different models for free-stream

https://doi.org/10.1017/S0022112008004345 Published online by Cambridge University Press

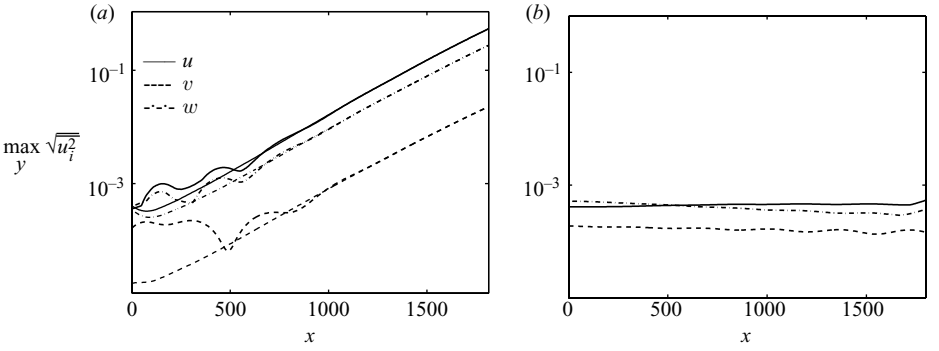


FIGURE 11. (*a*) Response of the non-parallel three-dimensional boundary layer to free-stream vorticity. Thick lines: spatial evolution of the boundary-layer disturbance, excited by a continuous Orr–Sommerfeld mode ($\omega = -0.01$, $\beta = -0.14$, $\gamma = 0.126$) at $Re_{\delta^*} = 220$. Thin lines: spatial evolution of the corresponding crossflow instability wave. (*b*) Response of a parallel Falkner–Skan–Cooke boundary layer at $Re_{\delta^*} = 360$ to a continuous Orr–Sommerfeld mode ($\omega = -0.01$, $\beta = -0.14$, $\gamma = 0.126$).

vorticity have been employed: streamwise vortices by Bertolotti (1997) and Bertolotti & Kendall (1997), oblique waves by Berlin & Henningson (1999) and eigenmodes from the continuous spectrum of the Orr–Sommerfeld/Squire operator by e.g. Jacobs & Durbin (2001), Brandt *et al.* (2002, 2004) and Zaki & Durbin (2005). In all cases, the receptivity process was characterized by the formation of streamwise elongated structures, referred to as streaks, while the excitation of TS waves was bypassed. The streaks are not eigenmodes of the base flow and undergo algebraic instead of exponential growth.

In this paper, we investigate the receptivity mechanism to free-stream vorticity in the three-dimensional swept-plate boundary layer. Figure 11(*a*) shows the evolution of the boundary-layer disturbance, when a continuous Orr–Sommerfeld mode is prescribed at the inflow plane of the computational domain. A transient region can be identified up to $x \simeq 1000$, whereas further downstream, the evolution of the boundary-layer disturbance is fully determined by exponential growth of unsteady crossflow instability. Hence, the swept-plate boundary layer supports receptivity for travelling crossflow modes to free-stream vortices. From figure 10, it is clear that there is no location where the wavenumbers of free-stream disturbance and unstable eigenmode match. Wavenumber reduction from the forcing wavenumber α_{FS} to the eigenmode wavenumber α_{CF} through chordwise mean-flow variations is thus a requirement for the excitation of the observed crossflow instability.

The upstream transient growth of the boundary-layer disturbance in figure 11(*a*) is mainly due to the forcing of Squire modes by the Orr–Sommerfeld free-stream mode, as also seen in Zaki & Durbin (2005). These are all stable but non-normal, thus giving rise to non-modal growth. Some transient behaviour might also result from the fact that the free-stream modes are eigenmodes of the Orr–Sommerfeld/Squire operator, which might cause some initial adjustment to the non-parallel mean flow. We performed tests on domains with different lengths of the fringe region and heights of the free stream. This had small effects on the adjustment of the free-stream mode, and we found that the growth of the unstable eigenmode was hardly affected.

The significance of the strongly non-parallel upstream region of the three-dimensional base flow for the receptivity due to free-stream vorticity becomes evident through figure 11(*b*). This plot shows the response of the parallel Falkner–Skan–Cooke

https://doi.org/10.1017/S0022112008004345 Published online by Cambridge University Press

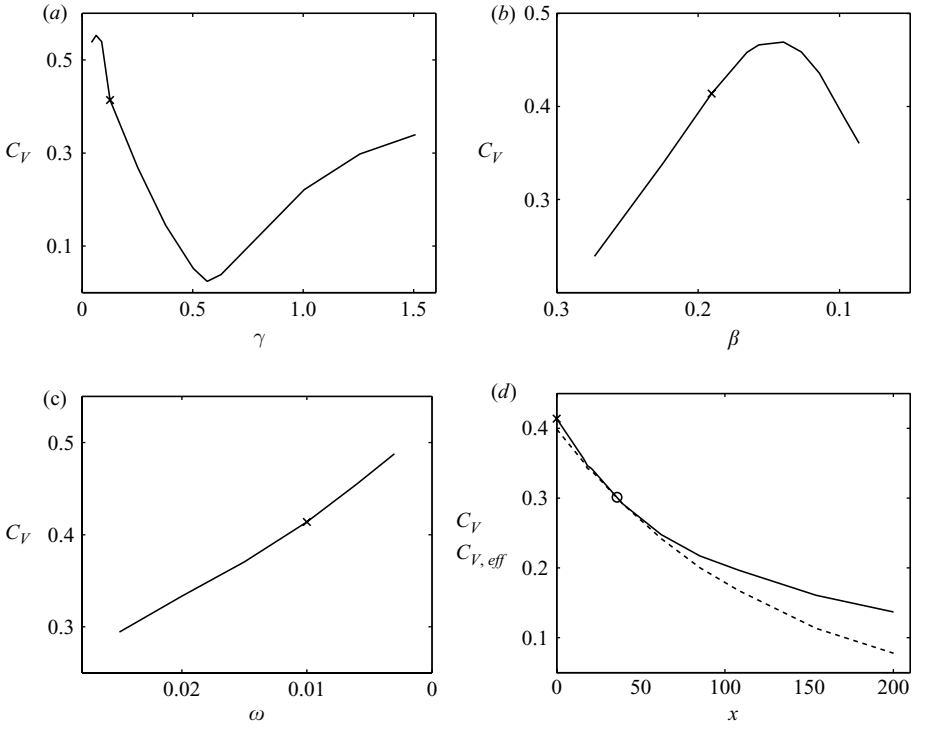


FIGURE 12. Dependence of the receptivity coefficient to free-stream vorticity on (*a*) the wall-normal wavenumber, (*b*) the spanwise wavenumber and (*c*) the angular frequency of the vortical mode. In (*d*), the influence of the chordwise station on C_V is shown, at which the free-stream disturbance is prescribed (——). Effective receptivity coefficient (---). ○, the first neutral point of the excited unsteady crossflow mode. The plots are based on $(Re_\delta, \omega; \beta, \gamma) = (220, -0.01; -0.19, 0.126)$, marked by the cross.

boundary layer to forcing with a free-stream vortical mode at an unstable Reynolds number, and the result is obtained by means of DNS of the parallel mean flow. Clearly, no unstable crossflow wave is excited, that is, removing the non-parallel nature of the base flow deactivates the unsteady receptivity mechanism seen in figure 11(*a*). This observation also confirms that the required length-scale conversion discussed in the previous subsection is only supported in the spatially developing flow.

The receptivity mechanism for travelling crossflow instability is quantified in terms of the receptivity coefficient $C_V = C_V(\beta, \omega; m, \phi_0)$,

$$C_V = \frac{A_R}{\varepsilon_v}, \tag{4.3}$$

where A_R is the receptivity amplitude of the excited unsteady crossflow wave, and ε_v is the maximum amplitude of the vortical free-stream mode, assumed to be small. Both amplitudes are taken at the inflow plane of the domain, where the free-stream mode is prescribed. They are measured in terms of the wall-normal maximum of $\sqrt{\overline{u^2}}$. Figure 12(*a*) shows the influence of the wall-normal wavenumber, figure 12(*b*) the spanwise wavenumber and figure 12(*c*) the angular frequency of the Orr–Sommerfeld free-stream mode on the receptivity coefficient. The vortical disturbance is computed at $Re_{\delta *} = 220$. Figure 12(*d*) displays the dependence of C_V on the chordwise station, at which the vortical mode is introduced in the free stream.

https://doi.org/10.1017/S0022112008004345 Published online by Cambridge University Press

Figure 12(*a*) shows that receptivity is most efficient for free-stream modes with a large wall-normal length scale. The maximum in C_V is obtained at $\gamma = 0.063$. This corresponds to a normal scale of $\lambda_y = 30.44$ times the 99 % boundary-layer thickness at the inflow plane. Large receptivity coefficients are also observed in the range of small values for λ_y, namely at $\gamma = 1.508$ ($\lambda_y = 1.27$ inlet 99 %-thicknesses), where $C_V > 0.3$. In contrast, C_V drops down to almost zero for the intermediate scales. Comparison with figure 9(*c*) suggests that the receptivity mechanism is most efficient for vortical free-stream modes of either low decay rate or large penetration depth. On the other hand, typical energy spectra for turbulent fields reveal that turbulent kinetic energy is concentrated on the small wavenumbers. Hence, the deeply penetrating vortical modes of large γ might in practice be unimportant for the transition process, in spite of the rather large receptivity coefficients associated with them. In figure 12(*b*), an optimal spanwise wavenumber of $\beta = -0.14$ can be identified, at which C_V is maximum. Compare with steady receptivity to surface roughness, § 3.1, being most efficient at $\beta = -0.19$.

Figure 12(*c*) shows that the efficiency of the receptivity process increases when ω approaches zero. The figure is restricted to the negative ω half-plane, where the unstable crossflow modes are found. Inspection of figure 9(*b*) reveals that the increase of C_V for $\omega \to 0$ can again be attributed to a large penetration depth. Also Jacobs & Durbin (1998) found maximum receptivity in Blasius flow for the deeply penetrating vortical modes of low frequency. Figure 12(*d*) displays the dependence of C_V on the chordwise station, where the free-stream mode is prescribed. This location is equivalent with the inflow plane. Hence, various domains with different inflow Reynolds numbers $Re_{\delta*,0}$ are used for this study, and the vortical mode is computed at the according inflow Reynolds number. The origin in the figure complies with $Re_{\delta*,0} = 220$. As in figure 6, it is again meaningful to consider the effective receptivity coefficient,

$$C_{V,eff} = \frac{C_V}{e^{N_R}} = C_V \frac{A_I}{A_R} = \frac{A_I}{\varepsilon_v}, \tag{4.4}$$

to take the decay or growth of the crossflow instability at the inflow plane into account. N_R is the N-factor of the unsteady crossflow mode at the inlet and A_I is its amplitude at the first neutral point. Clearly, receptivity to free-stream vorticity is most efficient at $x = 0$ ($Re_{\delta*,0} = 220$) where the boundary layer is thin and highly non-parallel. The same result has been obtained in figure 6 for steady receptivity to surface roughness. It can be concluded that the scale-conversion process required for receptivity is most efficient in the rapidly evolving region near the leading edge. However, the curves in figure 12(*d*) suggest that even larger receptivity coefficients can be expected upstream of $Re_{\delta*,0} = 220$ in the immediate vicinity of the leading edge. These receptivity sites cannot, however, be addressed by the present numerical method.

In summary, the unsteady receptivity mechanism due to vortical free-stream modes herein proposed has characteristics in common with both the localized and non-localized receptivity processes so far discussed in literature. On the one hand, the vortical disturbance resides in the entire free stream and acts non-locally on the boundary layer. In contrast to Blasius flow, on the other hand, where the excitation of streak-like disturbances inside the boundary layer is non-localized, the present mechanism for unsteady crossflow modes in three-dimensional flow is efficient only near the leading edge. In this limited region, the basic flow is sufficiently non-parallel

https://doi.org/10.1017/S0022112008004345 Published online by Cambridge University Press

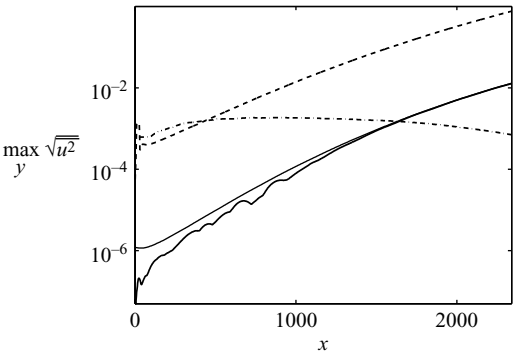


FIGURE 13. Combination of free-stream vorticity and surface roughness. The roughness element ($\beta_R = 0.190$) excites an unstable steady eigenmode (---), while the vortical free-stream mode ($\beta_V = -0.381$) does not trigger a growing travelling mode (-·-). In combination, however, they excite travelling crossflow instability (——, thick curve).

to provide the length scale of the crossflow instability through scale conversion. This is a characteristic of localized receptivity.

5. Combination of roughness and free-stream vorticity

In the presence of both surface roughness and free-stream turbulence, stationary and travelling crossflow modes will coexist in three-dimensional boundary layers and compete with each other. This situation is modelled here by considering the combination of a spanwise periodic localized roughness element on the plate and a vortical Orr–Sommerfeld mode in the free stream, both assumed to have small amplitudes. In §§ 3 and 4, it was demonstrated that there exists a direct receptivity mechanism to localized roughness and vortical free-stream disturbances, causing the occurrence of stationary and travelling crossflow modes in the boundary layer. These mechanisms will still be present in the case of combined surface roughness and free-stream vorticity. Both the steady and the unsteady receptivity process may then give amplifying eigenmodes, which interact continuously and force a wavelike disturbance. This process thus builds on the combination of the two direct receptivity mechanisms discussed in the previous sections, followed by nonlinear interaction.

Next, we examine whether there exists also a receptivity mechanism based on scattering of free-stream vorticity at the roughness in boundary layers of the Falkner–Skan–Cooke type. For this purpose, the mean flow is exposed to a vortical mode of spanwise wavenumber $\beta_V = -0.381$ together with a roughness element with $\beta_R = 0.190$. The response of the base flow is plotted in figure 13. While a stationary crossflow mode evolves from the steady disturbance field due to the roughness (dashed line), no unstable travelling crossflow wave is excited by this particular free-stream mode (dashed-dotted line). Unsteady crossflow instability is nevertheless observed in figure 13 (solid line), as deduced by comparing with the evolution curve for the travelling crossflow wave at $\beta_{CF} = -0.190$ (thin solid line). The unsteady crossflow mode is thus triggered by the interaction between the growing steady disturbance field caused by the roughness and the decaying unsteady perturbation due to the vortical free-stream disturbance. The spanwise wavenumber of the travelling eigenmode is given by $\beta_{CF} = \beta_V + \beta_R$, the frequency ω is provided by the free-stream disturbance, and the chordwise wavenumber α_{CF} by the roughness contour. Hence, the roughness

https://doi.org/10.1017/S0022112008004345 Published online by Cambridge University Press

element is responsible for the scale-enhancement process. To conclude, a receptivity mechanism for travelling crossflow instability has been identified, linearly depending on the amplitudes of both the free-stream vorticity and the surface roughness. It can be seen as the crossflow counterpart of the classical mechanism for Tollmien–Schlichting instability in Blasius flow proposed by Goldstein (1985) and Ruban (1985), which builds on the scattering of acoustic free-stream disturbances at localized surface roughness.

5.1. *Receptivity coefficient*

The receptivity mechanism shown in figure 13 and explained in the previous section results in the excitation of a travelling unstable eigenmode of the base flow. It can be quantified in terms of a receptivity coefficient,

$$C_{VR} = \frac{A_R}{\varepsilon_v \varepsilon_h H(\alpha_{CF})}, \tag{5.1}$$

where A_R is the receptivity amplitude of the excited travelling crossflow wave at the roughness station, and ε_v and ε_h are the amplitudes of the vortical free-stream disturbance and the roughness element. $H(\alpha_{CF})$ is the Fourier component of the roughness bump at the wavenumber of the steady disturbance. Equation (5.1) is analogous to the efficiency coefficient for receptivity to free-stream sound in combination with roughness, as used e.g. by Crouch (1993) and Choudhari (1994) for finite Reynolds-number theory calculations in Falkner–Skan–Cooke flow.

5.2. *Results*

The spanwise wavenumber β_{CF} of the travelling crossflow wave excited via the combination of roughness and free-stream vorticity is obtained through the sum of the wavenumbers β_V and β_R of the interacting unsteady and steady disturbance,

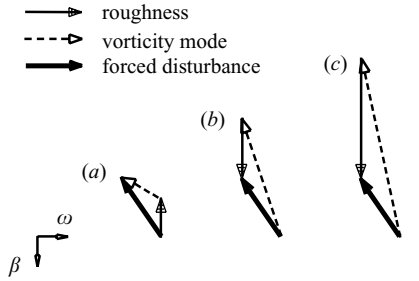
$$\beta_{CF} = \pm\beta_V \pm \beta_R, \tag{5.2}$$

i.e. four different unsteady waves per (β_V, β_R) combination can be forced at second order. In principle, an infinite number of such combinations may be considered. Here, ω, β_V and β_R are chosen to keep the frequency and spanwise scale of the generated mode constant and to examine the efficiency of the receptivity process when varying the spanwise scale of free-stream mode and roughness. In figure 14, three (β_V, β_R) combinations are reported, all summing to $\beta_{CF} = -0.190$. The specific summation of β and ω is highlighted by the arrow diagrams in figure 14. In the table, the receptivity coefficient C_{VR} is compiled. The largest coefficient is obtained in case (*a*), when the spanwise wavenumber of the free-stream mode is a third and that of the roughness element is two-thirds of the instability wavenumber β_{CF}. For case (*c*), the receptivity process is one order-of-magnitude weaker, showing that the difference between the forcing wavenumbers, β_V and β_R, and the forced wavenumber β_{CF} should not be too large.

In figure 15, the receptivity coefficient C_{VR} is plotted versus the chordwise station. The effective receptivity coefficient is again shown. Case (*b*) in figure 14 is considered here. Like the direct receptivity mechanisms for steady and unsteady crossflow modes, the receptivity process due to a combination of free-stream vorticity and roughness becomes most efficient in the region between the leading edge of the plate and the first neutral point of the excited travelling crossflow wave.

It has been shown above that unstable tra velling disturbances can occur, even if the unsteady forcing does not contain any unstable wavenumbers. Another scenario builds

https://doi.org/10.1017/S0022112008004345 Published online by Cambridge University Press



	(a)	(b)	(c)
ω	–0.01	–0.01	–0.01
β_V	–0.063	–0.381	–0.571
β_R	0.127	0.190	0.381
β_{CF}	–0.190	–0.190	–0.190
C_{VR}	0.109	0.067	0.013

FIGURE 14. Interaction between a decaying unsteady disturbance due to free-stream vorticity and an amplifying steady disturbance caused by localized roughness. Three combinations of the spanwise wavenumbers β_V and β_R of the vortical mode and the roughness element are considered. Excitation of an unstable travelling crossflow mode with spanwise scale $\beta_{CF} = -0.190$.

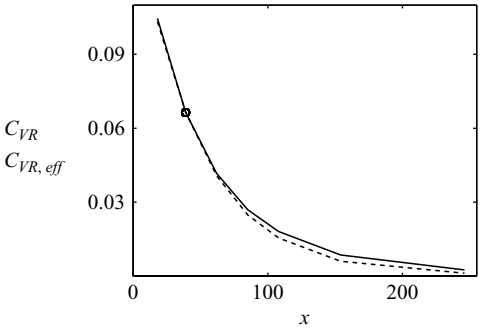


FIGURE 15. Coefficient for receptivity to free-stream vorticity combined with surface roughness versus chordwise location (——) and effective receptivity coefficient (---). The spanwise wavenumbers of the vortical mode and the roughness element are $|\beta_V| = 0.381$ and $\beta_R = 0.190$ (case (*b*) in figure 14). Circle: First neutral point of the excited unsteady crossflow wave.

on coexisting unstable stationary and travelling crossflow modes forcing an unsteady disturbance wave by interaction. This is then not a receptivity process on its own, but a combination of the two direct receptivity mechanisms, followed by interaction between the triggered instability waves. Such a situation is displayed in figure 16, where the forced wave (solid line) has again a wavenumber of $\beta = -0.190$. The chordwise wavenumber $\mathrm{Re}\{\alpha\}$ and the growth rate $\mathrm{Im}\{\alpha\}$ of this wave are obtained as the sum of the chordwise wavenumbers and growth rates of the interacting crossflow modes. This explains why the growth rate of the induced wave is larger than that of the unstable crossflow mode with the same spanwise wavenumber and frequency figure (13). Modes continuously forced by two unstable waves are therefore expected to have a large influence during the transition process. Both mechanisms, the excitation of unsteady crossflow instability and the forcing of travelling waves by interacting crossflow modes, need to be addressed in three-dimensional boundary layers.

6. Steady versus unsteady cross-flow instability

An important issue of receptivity and instability studies in three-dimensional boundary-layer flow is to determine whether stationary or travelling crossflow vortices

https://doi.org/10.1017/S0022112008004345 Published online by Cambridge University Press

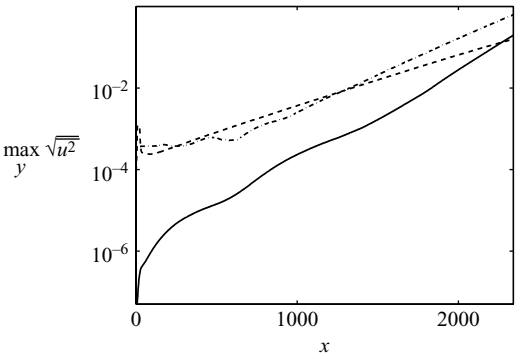


FIGURE 16. Combination of free-step vorticity and surface roughness. Both the roughness element ($\beta_R = 0.095$, ---) and the vortical free-stream mode ($\beta_V = -0.095$, ---) excite unstable crossflow eigenmodes, which interact and force a harmonic wave with $\beta_f = -0.190$ (——).

External perturbation	Receptivity mechanism	Excited disturbance	$\tilde{C}$	$\tilde{C}_{710}$
Roughess	Direct	Steady CF mode	0.221	2.27
Vorticity mode	Direct	Unsteady CF mode	0.469	10.54
Vorticity mode + roughness	Coupling	Unsteady CF mode	1.784	44.22

TABLE 3. Receptivity mechanisms for steady and unsteady crossflow (CF) instability and their efficiency. Amplitude coefficients at the receptivity site ($\tilde{C}$) and at $x = 710$ ($\tilde{C}_{710}$).

dominate the disturbance environment inside the boundary layer, see for example Saric *et al.* (2003). In §§ 3 to 5, three receptivity mechanisms for steady and unsteady crossflow instability have been investigated. Their efficiency has been quantified in terms of the receptivity coefficients C_R, C_V and C_{VR}, equations (3.1), (4.3) and (5.1), which can be used to assess the initial amplitude of the disturbance. In contrast to C_V, C_R and C_{VR} involve the spectral amplitude $H(\alpha)$ of the roughness shape. In order to compare the receptivity amplitudes A_R of the excited steady and unsteady crossflow instabilities, it is therefore convenient to re-formulate the receptivity coefficients of the three studied mechanisms in terms of a coefficient $\tilde{C}$,

$$\tilde{C}_R = \frac{A_R}{\varepsilon_h} = H(\alpha_{CF})C_R, \tag{6.1a}$$

$$\tilde{C}_V = \frac{A_R}{\varepsilon_v} = C_V, \tag{6.1b}$$

$$\tilde{C}_{VR} = \frac{A_R}{\varepsilon_v \varepsilon_h} = H(\alpha_{CF})C_{VR}. \tag{6.1c}$$

Table 3 compiles the three receptivity processes and the largest associated coefficients $\tilde{C}$. The maximum in $\tilde{C}_R$ is obtained for a roughness element of shape I and a spanwise wavenumber of $\beta_R = 0.157$. $\tilde{C}_V$ is largest for a free-stream mode of $\beta_V = -0.14$. The coefficient $\tilde{C}_{VR}$ for receptivity due to coupling at roughness is maximum, when a roughness element of $\beta_R = 0.127$ is combined with a free-stream mode of $\beta_V = -0.063$.

Whether steady or unsteady crossflow instability is dominant at the receptivity site will depend on the relative amplitude of the wall roughness and the vortical free-stream

https://doi.org/10.1017/S0022112008004345 Published online by Cambridge University Press

mode. In the following discussion, it is assumed that the amplitude of the roughness element is $\varepsilon_h = 0.025$, i.e. 2.5 % of the boundary-layer displacement thickness at the inflow plane and about 2.4 % of the local displacement thickness at the roughness station. This value corresponds approximatively to a roughness height of $k = 6\,\mu$m, as in the experiments by Reibert *et al.* (1996). Such a roughness bump will excite a steady crossflow mode with an initial amplitude of $A_R = \varepsilon_h \tilde{C}_R = 5.53 \times 10^{-3}$. A travelling crossflow wave of the same amplitude is obtained via direct receptivity, if a free-stream vortex with amplitude $\varepsilon_v = A_R/\tilde{C}_V = 0.012$ acts on the boundary layer. To obtain $A_R = 5.53 \times 10^{-3}$ via the mechanism due to unsteady disturbance scattering at the roughness, a free-stream mode with amplitude $\varepsilon_v = A_R/(\varepsilon_h \tilde{C}_{VR}) = 0.124$ must interact with the roughness-induced steady disturbance. Two conclusions can be drawn. (i) Direct unsteady receptivity for travelling crossflow instability is about ten times more efficient than unsteady receptivity to free-stream vorticity scattered at roughness of $\varepsilon_h = 0.025$ ($\simeq 6\,\mu$m) height. (ii) Given $\varepsilon_h = 0.025$, stationary crossflow modes will dominate at the receptivity site as long as the vortical free-stream disturbance has an amplitude lower than $\varepsilon_v = 1.2$ % of the chordwise free-stream velocity.

The dominating crossflow modes at the receptivity site are not necessarily the most dangerous instability waves further downstream. To estimate the relevant disturbances in the region of linear growth, the downstream amplitudes of the different instability waves have to be compared with each other, thus accounting for the initial amplification of the different unstable waves. Here, the comparison is performed at the position $x = 710$, which corresponds approximately to the second measurement station in Reibert *et al.* (1996). Amplitude coefficients in analogy with (6.1) are used by replacing the receptivity amplitude A_R by the wave amplitude at $x = 710$, A_{710}. They are denoted $\tilde{C}_{710}$ and given in the last column of table 3. Note that $\tilde{C}_{710}$ is largest for roughness of $\beta_R = 0.217$ and for free-stream vorticity of $\beta_V = -0.190$, i.e. spanwise wavenumbers other than those at the receptivity site are dominant at $x = 710$. The comparison of the downstream disturbance amplitudes leads to the following conclusions. (i) The stationary crossflow mode caused by $6\,\mu$m roughness amplifies to $A_{710} = \varepsilon_h \tilde{C}_{R,710} = 0.057$. Travelling crossflow instability excited via the direct receptivity process reaches the same amplitude at $x = 710$, when free-stream vorticity with $\varepsilon_v = A_{710}/\tilde{C}_{V,710} = 5.38 \times 10^{-3}$ acts on the boundary layer. (ii) The receptivity process for free-stream vorticity combined with roughness requires a continuous-spectrum mode with $\varepsilon_v = A_{710}/(\varepsilon_h \tilde{C}_{VR,710}) = 5.13 \times 10^{-2}$ and can again not compete with the direct receptivity mechanism. Also, continuous forcing of a non-modal wave by interacting crossflow instability, briefly mentioned at the end of § 5, is not relevant at $x = 710$, since a free-stream vortex with $\varepsilon_v = 8.63$ % would be required to obtain $A_{710} = 0.057$.

For the roughness considered above, the amplitude of the disturbance is still relatively low at $x = 710$, namely $\simeq 6$ % of the free-stream velocity. Further downstream, the competition between the stationary and the travelling crossflow modes can lead to different results, since unsteady crossflow modes amplify at larger growth rates than steady crossflow waves. Therefore, lower free-stream turbulence intensities than those estimated above can lead to a transition scenario dominated by travelling crossflow modes. Also the wave forced by interaction between two unstable modes grows faster than the stationary crossflow modes. To summarize, in the presence of micrometre-sized roughness, steady crossflow instability will dominate in the boundary-layer region up to $x = 710$, unless the free-stream disturbances have amplitudes of more than $\simeq 0.5$ % of the free-stream velocity.

https://doi.org/10.1017/S0022112008004345 Published online by Cambridge University Press

7. Conclusions

Receptivity of the three-dimensional boundary layer developing on a swept flat plate is investigated by direct numerical simulation. The ability of wall roughness, free-stream vortical modes and their interaction to trigger steady and travelling crossflow modes is shown. The base flow, solution to the Navier–Stokes equations with Falkner–Skan–Cooke profiles as the initial condition, is chosen with a sweep angle of 45° and a Hartree parameter $\beta_H = 0.33$ defining the free-stream acceleration.

Receptivity of steady crossflow vortices to localized spanwise periodic roughness elements is examined first. Our results reproduce the main features of previous studies in literature: roughness forces directly the unstable steady eigenmodes inside the boundary layer, and receptivity increases when the surface roughness is located upstream of the neutral stability points. In this work, the focus is on the validity of the local approximation for non-parallel flows, which is based on the assumption that receptivity is proportional to the spectral content of the roughness shape at the chordwise instability wavenumber. This enables the definition of receptivity coefficients independent of the particular shape of the roughness element. The present results show that this approximation is valid as long as the chordwise extension of the roughness is smaller than the wavelength of the unstable mode. For less localized roughness, the receptivity process becomes dependent on the shape of the roughness element. However, a first-order correction can be introduced as in Bertolotti (2000); this amounts to a second receptivity coefficient which multiplies the derivative of the spectral shape of the roughness $H'(\alpha)$. This contribution is almost zero for very localized roughness elements, characterized by flat Fourier transforms with $H'(\alpha) \approx 0$, and significant for waves not represented by the roughness shape, $H(\alpha) \approx 0$, i.e. waves shorter than the characteristic chordwise length of the surface irregularity. However, we found that the correction after Bertolotti (2000) gives roughness-shape independent receptivity coefficients only within a limited range of chordwise bump lengths.

The influence of bump height on receptivity has been presented, as well. For the roughness elements under consideration, it has been shown that nonlinear effects on receptivity come into play beyond a bump amplitude of about 5 % of the displacement thickness, leading to slowly decreasing efficiency coefficients as the roughness height is increased. Nonlinearity has, however, a weaker effect on receptivity than on the subsequent growth of the unstable crossflow mode.

Free-stream vortical modes impinging on a three-dimensional boundary layer are modelled by the continuous-spectrum eigenmodes of the linearized Orr–Sommerfeld/Squire operator. To the best of our knowledge, the modes pertaining to the three-dimensional base flow are examined for the first time in this work. The three-dimensional base flow is shown to cause a significantly larger damping of the continuous modes towards the wall, which are therefore confined outside the shear layer. Unlike in two-dimensional boundary layers, the most penetrating modes are found to be quasi-two-dimensional waves, with very small values of the spanwise wavenumber. This can be explained by the fact that two-dimensional waves become insensitive to the spanwise (or crossflow) velocity component. These modes are also associated with low values of the chordwise wavenumber, and therefore represent large horizontal structures with scales much larger than those of the unstable waves.

The direct receptivity mechanism in the presence of free-stream modes is entirely due to the non-parallel nature of the base flow. This provides the streamwise variations necessary for the scale-conversion process, by which the unstable crossflow modes

https://doi.org/10.1017/S0022112008004345 Published online by Cambridge University Press

are excited. Free-stream modes have also been used previously to investigate the receptivity of two-dimensional boundary-layer flows, where they are shown to trigger significant transient growth of low-frequency modes. However, this is not observed in the present case. This can be explained by the presence of strong inflectional instabilities in three-dimensional boundary layers, and by the favourable pressure gradient, reducing transient effects.

The efficiency of receptivity to free-stream vorticity is measured in terms of a receptivity coefficient, defined by the ratio between the initial amplitude of the unstable travelling mode and the level of fluctuations in the free stream. The magnitude of the receptivity coefficient is determined by two competing effects. On the one hand, modes with fast variations in the wall-normal direction experience larger decay rate in the chordwise direction and are therefore less effective in forcing the boundary layer along significant chordwise distances. At the same time, these modes are less sheltered by the mean shear and have therefore larger support inside the boundary layer. The three-dimensional base flow has been shown to be receptive to both deeply penetrating vortical modes with small wall-normal scale and slowly decaying modes with large normal length scale. The results also demonstrate that the scale conversion of the free-stream mode is more efficient at lower Reynolds numbers, i.e. where the streamwise variations of the base flow are more significant. This points to the need for correct modelling of leading-edge effects in order to capture the initial entrainment of the free-stream modes.

The coupling between steady perturbations excited by wall roughness and unsteady disturbances induced by free-stream vorticity is also investigated. The results indicate that the stationary and travelling modes can efficiently force a wave with the frequency of the external vortical disturbance and a spanwise wavenumber given by the sum of those of the generating modes. If the two interacting modes are both unstable, they continuously force an unsteady wave amplifying at a rate equal to the sum of the growth rates of the interacting parent modes. On the other hand, modal travelling crossflow instability is observed when the vortical free-stream mode cannot directly trigger an unsteady growing disturbance, showing also that a receptivity mechanism related to the scattering of free-stream modes on the roughness surface is available. However, the receptivity coefficients related to this receptivity process are much smaller than for the mechanism in the absence of roughness. Travelling crossflow instability is therefore triggered via direct receptivity to free-stream vorticity in low-noise environments.

The relative importance of the two direct receptivity mechanisms is estimated by considering a roughness height of the order of 2.5 % of the boundary-layer displacement thickness. It is found that steady crossflow instability will dominate in the boundary layer, unless the free-stream disturbances have amplitudes of about $\simeq 0.5\,\%$ of the free-stream velocity. Note that the latter estimate can be considered conservative for the travelling modes since it is based only on the initial growth of the unstable waves.

The receptivity mechanisms due to coupling of free-stream modes at roughness presented in this work may become important at high levels of free-stream turbulence. In this case, we should also consider the nonlinear interaction among free-stream modes. This type of interaction is found to be the dominant mechanism in the case of streaks forced in the Blasius boundary layer by free-stream turbulence intensities larger than 3.5 % (see Brandt *et al.* 2004). In three-dimensional boundary layers, we can expect an even larger relevance of these nonlinear effects; in this case, the interaction between two exponentially growing modes may continuously induce

https://doi.org/10.1017/S0022112008004345 Published online by Cambridge University Press

waves with large amplification and quickly create a disturbed boundary-layer flow. To analyse this scenario better, full nonlinear simulations are the most suitable tool, and future work is planned in this direction.

This research is supported by VR (The Swedish Research Council). SNIC computing facilities located at the Center for Parallel Computers (PDC), KTH, have been used for parts of the computations.

REFERENCES

Berlin, S. & Henningson, D. S. 1999 A nonlinear mechanism for receptivity of free-stream disturbances. *Phys. Fluids* **11**, 3749–3760.

Bertolotti, F. P. 1997 Response of the Blasius boundary layer to free-stream vorticity. *Phys. Fluids* **9**, 2286–2299.

Bertolotti, F. P. 2000 Receptivity of three-dimensional boundary-layers to localized wall roughness and suction. *Phys. Fluids* **12** (7), 1799–1809.

Bertolotti, F. P. & Kendall, J. M. 1997 Response of the Blasius boundary layer to Controlled free-stream vortices of axial form. *AIAA Paper* 97-2018.

Bippes, H. & Deyhle, H. 1992 Das receptivity-problem in Grenzschichten mit längswirbelartigen Störungen. *Z. Flugwiss. Weltraumforschung* **16**, 34–41.

Brandt, L., Henningson, D. S. & Ponziani, D. 2002 Weakly non-linear analysis of boundary layer receptivity to free-stream disturbances. *Phys. Fluids* **14**, 1426–1441.

Brandt, L., Schlatter, P. & Henningson, D. 2004 Transition in boundary layers subject to free-stream turbulence. *J. Fluid Mech.* **517**, 167–198.

Buter, T. A. & Reed, H. L. 1994 Boundary layer receptivity to free-stream vorticity. *Phys. Fluids* **6** (10), 3368–3379.

Chevalier, M., Schlatter, P., Lundbladh, A. & Henningson, D. S. 2007 A pseudo-spectral solver for incompressible boundary layer flows. *Tech. Rep.* TRITA-MEK 2007:07. Royal Institute of Technology (KTH), Dept of Mechanics, Stockholm.

Choudhari, M. 1994 Roughness-induced generation of crossflow vortices in three-dimensional boundary layers. *Theor. Comput. Fluid Dyn* **6**, 1–30.

Choudhari, M. & Streett, C. L. 1992 A finite Reynolds number approach for the prediction of boundary layer receptivity in localized regions. *Phys. Fluids* A **4**, 2495–2514.

Collis, S. S. & Lele, S. K. 1999 Receptivity to surface roughness near a swept leading edge. *J. Fluid Mech.* **380**, 141–168.

Crouch, J. D. 1992 Localized receptivity of boundary layers. *Phys. Fluids* A **4** (7), 1408–1414.

Crouch, J. D. 1993 Receptivity of three-dimensional boundary layers. *AIAA Paper* 93-0074.

Crouch, J. D. & Spalart, P. R. 1995 A study of non-parallel and nonlinear effects on the localized receptivity of boundary layers. *J. Fluid Mech.* **290**, 29–37.

Fransson, J. H. M., Matsubara, M. & Alfredsson, P. H. 2005 Transition induced by free-stream turbulence. *J. Fluid Mech.* **527**, 1–25.

Goldstein, M. E. 1983 The evolution of Tollmien–Schlichting waves near a leading edge. *J. Fluid Mech.* **127**, 59–81.

Goldstein, M. E. 1985 Scattering of acoustic waves into Tollmien–Schlichting waves by small streamwise variations in surface geometry. *J. Fluid Mech.* **154**, 509–529.

Grosch, C. E. & Salwen, H. 1978 The continuous spectrum of the Orr–Sommerfeld equation. Part 1. The spectrum and the eigenfunctions. *J. Fluid Mech.* **87**, 33–54.

Högberg, M. & Henningson, D. 1998 Secondary instability of cross-flow vortices in Falkner–Skan–Cooke boundary layers. *J. Fluid Mech.* **368**, 339–357.

Jacobs, R. G. & Durbin, P. A. 1998 Shear sheltering and continuous spectrum of the Orr–Sommerfeld equation. *Phys. Fluids* **10** (8), 2006–2011.

Jacobs, R. G. & Durbin, P. A. 2001 Simulations of bypass transition. *J. Fluid Mech.* **428**, 185–212.

Kendall, J. M. 1998 Experiments on boundary-layer receptivity to freestream turbulence. *AIAA Paper* 98-0530.

https://doi.org/10.1017/S0022112008004345 Published online by Cambridge University Press

Lin, N., Reed, H. & Saric, W. 1992 Effect of leading edge geometry on boundary-layer receptivity to freestream sound. In *Instability, Transition and Turbulence* (ed. M. Hussaini, A. Kumar & C. Streett). Springer.

Malik, M. R., Zang, T. A. & Hussaini, M. Y. 1985 A spectral collocation method for the Navier–Stokes equations. *J. Comput. Phys.* **61**, 64–88.

Maslowe, S. A. & Spiteri, R. J. 2001 The continuous spectrum for a boundary layer in a streamwise pressure gradient. *Phys. Fluids* **13** (5), 1294–1299.

Ng, L. L. & Crouch, J. D. 1999 Roughness-induced receptivity to crossflow vortices on a swept wing. *Phys. Fluids* **11** (2), 432–438.

Nordström, J., Nordin, N. & Henningson, D. S. 1999 The fringe region technique and the Fourier method used in the direct numerical simulation of spatially evolving viscous flows. *SIAM J. Sci. Comput.* **20**, 1365–1393.

Reibert, M. S., Saric, W. S., Carillo, R. B. & Chapman, K. L. 1996 Experiments in nonlinear saturation of stationary crossflow vortices in a swept-wing boundary layer. *AIAA Paper* 96-0184.

Ruban, A. I. 1985 On the generation of Tollmien–Schlichting waves by sound. *Fluid Dyn.* **19**, 709–716.

Saric, W. S., Reed, H. L. & Kerschen, E. J. 2002 Boundary-layer receptivity to freestream disturbances. *Annu. Rev. Fluid Mech.* **34**, 291–319.

Saric, W. S., Reed, H. L. & White, E. B. 2003 Stability and transition of three-dimensional boundary layers. *Annu. Rev. Fluid Mech.* **35**, 413–440.

Schlichting, H. 1979 *Boundary-Layer Theory*, 7th edn. McGraw-Hill.

Schmid, P. J. & Henningson, D. S. 2001 *Stability and Transition in Shear Flows*. Springer.

Zaki, T. A. & Durbin, P. A. 2005 Mode interaction and the bypass route to transition. *J. Fluid Mech.* **531**, 85–111.

Zaki, T. A. & Durbin, P. A. 2006 Continuous mode transition and the effects of pressure gradient. *J. Fluid Mech.* **563**, 357–388.

Zavol'skii, N. A., Reutov, V. P. & Ryboushkina, G. V. 1983 Generation of Tollmien–Schlichting waves via scattering of acoustic and vortex perturbations in boundary layer on wavy surface. *J. Appl. Mech. Tech. Phys.* **24**(3), 355–361.

https://doi.org/10.1017/S0022112008004345 Published online by Cambridge University Press